A STUDY IN DRAG REDUCTION OF CLOSE FORMATION FLIGHT ACCOUNTING FOR FLIGHT CONTROL TRIM POSITIONS AND DISSIMILAR FORMATIONS

THESIS

Michael T. Morgan, Major, USAF

AFIT/GAE/ENY/05-M13

DEPARTMENT OF THE AIR FORCE
AIR UNIVERSITY

AIR FORCE INSTITUTE OF TECHNOLOGY

Wright-Patterson Air Force Base, Ohio

The views expressed in this thesis are those of the author and do not reflect the official policy or position of the United States Air Force, Department of Defense, or the U.S. Government.

AFIT/GAE/ENY/05-M13

A STUDY IN DRAG REDUCTION OF CLOSE FORMATION FLIGHT ACCOUNTING FOR FLIGHT CONTROL TRIM POSITIONS AND DISSIMILAR FORMATIONS

THESIS

Presented to the Faculty

Department of Aeronautics and Astronautics

Graduate School of Engineering and Management

Air Force Institute of Technology

Air University

Air Education and Training Command

In Partial Fulfillment of the Requirements for the

Degree of Master of Science in Aeronautical Engineering

Michael T. Morgan, BS

Major, USAF

March 2005

AFIT/GAE/ENY/05-M13

A STUDY IN DRAG REDUCTION OF CLOSE FORMATION FLIGHT ACCOUNTING FOR FLIGHT CONTROL TRIM POSITIONS AND DISSIMILAR FORMATIONS

Michael T. Morgan, BS

Major, USAF

Approved:

/SIGNED/	02 Feb 05
David R. Jacques, PhD (Chairman)	Date
/SIGNED/	02 Feb 05
Bradley S. Liebst, PhD (Member)	Date
/SIGNED/	02 Feb 05
Russell G. Adelgren, PhD (Member)	Date

Acknowledgments

This thesis was a two and a half year endeavor that started at the Air Force Institute of Technology and ended at the USAF Test Pilot School. The work would not have been completed without the help of numerous individuals. In Ohio, the project originated with my thesis advisor, Dr. David Jacques, who steered me on course and scoped the research. Additionally, I was indebted to the help of Mr. William Blake, AFRL. His assistance with the computer programming was invaluable.

In California, Mr. Ed Haering of the National Aeronautics and Space Administration was instrumental in the relative positioning solution. He was influential in the determination of the GPS receivers to use and the antennae placement for the modification to the two aircraft. I was fortunate to work with an outstanding flight test team for the project at Test Pilot School. The efforts of Capt Jason Randall, Capt Alan Wigdahl, Capt Chris Snyder, Capt Andrew Wright, and Lt Javier Hurtado allowed for the completion of the flight test.

Finally, I was fortunate to have the support of my wife and children. Their sacrifices and support over the long road allowed me to spend time and effort on the completion of this project.

Table of Contents

Page

Page

Page

List of Figures

Page

Page

List of Tables

Page

List of Symbols and Abbreviations

AFB.....Air Force Base

AFIT.....Air Force Institute of Technology

AFRL .....Air Force Research Laboratory

AS .....Airspeed

b.....Wingspan

c.g.....Center of Gravity

C_D.....Drag Coefficient

C_L .....Lift Coefficient

C_l .....Roll Coefficient

C_n.....Yaw Coefficient

D.....Drag

DAS.....Data Acquisition System

DEEC .....Digital Electronic Engine Control

ECEF.....Earth-Centered, Earth Fixed

ENU .....East-North-Up

E_s .....Specific Energy

F_{ex}.....Excess Thrust

FF .....Fuel Flow

FS .....Fuel Savings

ft .....Feet

g.....Gravitational Constant

GPS .....Global Positioning System

HASC.....High Angle-of-Attack Stability and Control

hp.....Altitude

HVM .....Horseshoe Vortex Method

in .....inches

K_{xx}.....Induced Drag Correction Factor

KCAS.....Knots Calibrated Airspeed

KIAS .....Knots Indicated Airspeed

kts.....Knots

L .....Lift

NACA .....National Advisory Committee for Aeronautics

NASA.....National Aeronautics and Space Administration

NED .....north-East-Down

n_{FPA}.....Flight Path Acceleration

P_R.....Required Power

P_s .....Specific Excess Power

q.....Dynamic Pressure

R.....Ratio of Induced Drag Reduction

rpm .....Revolutions Per Minute

S .....Surface Area

s.....Seconds

TPS.....Test Pilot School

T_R .....Required Thrust

TSFC.....Thrust Specific Fuel Consumption

U.....Freestream Velocity

UAV.....Unmanned Aerial Vehicle

USAF .....United States Air Force

V.....Velocity

VISTA.....Variable Stability In-Flight Simulator Test Aircraft

VLM.....Vortex Lattice Method

W.....Weight

w.....Upwash Velocity

$\dot{w}_f$ .....Fuel Flow

x/b .....Normalized Longitudinal Spacing

y/b .....Normalized Lateral Spacing

z/b.....Normalized Vertical Spacing

Φ .....Roll Angle

Γ .....Circulation Strength

Θ.....Pitch Angle

Ψ .....Yaw Angle

α.....Angle of Attack

β .....Sideslip Angle

δ_a .....Combined Flaperon and Rudder Deflection Angle

δ_f.....Flaperon Deflection Angle

δ_r.....Rudder Deflection Angle

δ_s .....Horizontal Stabilator Deflection Angle

ρ .....Density

AFIT/GAE/ENY/05-M13

Abstract

This thesis further defines the position of greatest fuel savings benefit for the trail aircraft flying in a two-ship formation. The cooperative formation profile was similar to that of migratory birds and comparable methods were used for the analysis. The HASC95 vortex lattice code was used for the examination. A similar formation of F-16 aircraft and a dissimilar formation of a lead KC-135 aircraft and a trail F-16 aircraft were investigated. Both investigations trimmed the aircraft in the yaw and roll axes to determine the optimal savings. The similar analysis was conducted at an altitude of 20,000 feet and three airspeeds; cruise speed of 300 knots, maximum range airspeed of 271 knots, and maximum endurance airspeed of 211 knots. The savings for the trail aircraft were determined to be 16%, 21%, and 34%, respectively, at a constant wingtip overlap of 13.5% of the wingspan. The dissimilar formation was completed at an altitude of 20,000 feet and 300 knots airspeed. This resulted in a 26% savings for the trail aircraft with a wingtip overlap of 16.7% of its wingspan.

A flight test was flown for the similar formation profile. The flight test captured data for the mission at 300 knots. The results of the flight test were inconclusive. However, the determined area of apparent savings was bounded by 7.9% to 19.9% wingtip overlap and -3.2% to -7.3% vertical separation. At the bounds, fuel savings of 12% and 13% ±7% were observed.

The analytical study was accomplished at the Air Force Institute of Technology, Wright-Patterson AFB. The flight test was conducted at the USAF TPS, Edwards AFB, California. The flight test missions were flown in two USAF F-16 aircraft.

A STUDY IN DRAG REDUCTION OF CLOSE FORMATION FLIGHT ACCOUNTING FOR FLIGHT CONTROL TRIM POSITIONS AND DISSIMILAR FORMATIONS

I. Introduction

Modern formation flight is based on the concept of mutual support and strength in numbers. Traditional formation positions place a wingman as close to the lead aircraft as three feet wingtip separation and as far away as of two nautical miles. Close positions enhance the ability of the wingman to maintain visual contact with the lead and are readily used to penetrate weather and perform in show formations. Conversely, the extended lateral positions amplify the mobility of the formation and allow for increased offensive postures during a conflict. Recently, there has been resurgence in the study of reducing fuel consumption and thus effectively increasing the range of a formation by exploiting the wingtip vortices generated by the lead aircraft, thus decreasing the induced drag on the trail aircraft. This benefit will occur as a result of the trail aircraft flying in a region of upwash from the lead aircraft. No hardware modification is necessary to the airframe, and the direct savings in fuel consumption are without cost. A fighter-type formation would be able to increase its time aloft or range during a minimum-fuel scenario. Similarly, a formation of Unmanned Aerial Vehicles (UAV) flying in extended cruise with an aerial refueling aircraft would be able to conserve fuel and increase the

range of the formation. This would, of course, require the use of a station-keeping autopilot to preserve the ideal position.

Background

The concept of flying aircraft in a minimum drag formation profile was born from the observation of birds flying in formation. The rationale behind migratory bird formations has been theorized as twofold. First, by flying in formation birds are able to gain an aerodynamic advantage and thus reduce their energy expenditure. Second, the closer proximity of the members improves communication within the group (18:322-323). In an attempt to grasp an understanding of this phenomenon, a series of observations were conducted on great white pelicans (38:697-698). The experiment utilized specially trained pelicans to fly in a "V" formation. These birds were equipped with heart-rate monitors and were monitored by a moving motorboat and an ultra-light aircraft. Through this study, it was determined that birds flying in formation had heart rates 11.4% to 14.5% lower than birds flying a similar solo profile. A related study on pink-footed geese was conducted (11:253,255-256). This experiment focused on the formation spacing of the individual members and its relationship with the theoretical minimum drag spacing. During this study, several "V" formations of geese were photographed from directly below and measurements were taken to determine observed positions with the theoretical optimal spacing. For the geese, it was determined that the optimal spacing for the trailing birds should result in a 5% overlap of the wingspan,

determined from a horseshoe vortex analysis. However, the observed mean spacing of the formation showed roughly 15.5% wingtip separation of the geese. The reason for the difference from optimal spacing was theorized to be a result of the poor station-keeping ability of the birds. Flight inside of the optimal spacing resulted in an increase in required energy by placing the bird in a region of downwash. This suggests that if the errors in maintaining formation position are large, birds would tend to fly at a lesser wingtip overlap to avoid increasing the required energy. Nevertheless, even at this increased separation the formation of birds gain a benefit over the solo bird in flight. This has been determined through the modeling of various bird formations and analyzing the results.

The numerical representation of a formation is based on the application of Munk's Stagger Theorem (26:377). In application, the induced drag of the entire system is independent of the streamwise location of the spanloads, provided the circulation remains constant. Factors that affect the amount of drag reduction, and hence power reduction, are the number of bodies in the formation and the lateral separation of each of the bodies. If the formation is aligned in the unstaggered, line abreast position, there is a mutual and equal benefit to each member. While the induced drag of the system is unchanged by the introduction of stagger in the formation, the benefits to the individual members vary considerably (20:9). A trail body in the formation experiences a greater updraft from the preceding body, as compared to a line abreast formation. The application of this theorem to the formation flight profile will be discussed in detail in Chapter 2.

Utilizing this approach, Hummel has shown a significant improvement of 10% power reduction for a two-body formation of identical lifting surfaces, with no wingtip overlap (18:330-331). Hummel used the Horseshoe Vortex Method (HVM) reducing the wing surface to a representative horseshoe vortex approximately 78% of the span in width. Additionally, there was an energy savings increase by a factor of nearly three as the size of the formation approaches infinity. As the lateral distance increased between members, the induced drag and lift perturbations vanished, tending to zero at infinity, and hence the associated power reduction disappeared. This can be seen in Figure 1, where E is the total power reduction for the formation, $\Delta\eta$ is the lateral spacing normalized by the span, and n is the number of elements of the formation. A $\Delta\eta$ of zero indicates no wingtip overlap.

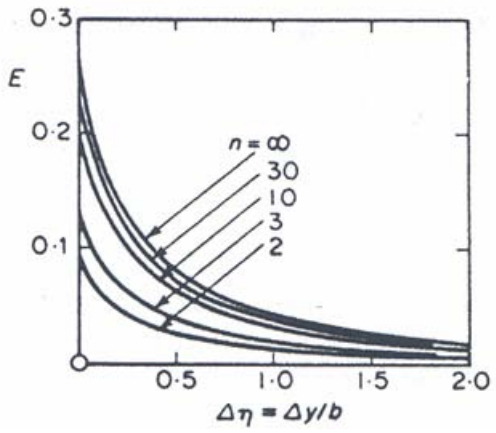

Figure 1. Predicted Energy Savings (18:331)

The actual shape of the formation plays an important role in the derived benefits. Through the application of a genetic algorithm, the optimal formation shape has been

shown to be a “V.” In the simulation of a flock of 300 American Blackpool Warblers, the system was allowed to randomly stagger for maximum benefit (16:6-7). The resulting geometry was a “V” formation that produced an 18.35% drag reduction as compared to a bird in solo flight.

Aerodynamic properties of migratory bird formations produce considerable benefits for the flocks. However, as seen in the observation studies, birds do not always fly in a region of maximum benefit. It appears that the natural tendency of different species of birds to migrate in formation is twofold, incorporating both increased communication and reduced drag benefits. Even though they are not receiving maximum induced drag savings at all times, by flying in a formation the birds are benefiting from the flock as a whole. The application of drag reduction and its direct relevance to a formation of aircraft is the focus of this thesis. As such, the exact reason as to a bird’s rationale is irrelevant.

Aircraft flying in a minimizing drag formation have the capability to reduce the fuel consumption or increase the range aloft. Unlike birds, which morph their wing shape to minimize spanwise loading, the geometry of an aircraft is fixed. However, similar to the analyses of birds, utilizing lifting line theory, the trailing wake of an aircraft can be reduced to a series of horseshoe vortices. A representation of the resultant areas associated with the upwash and downwash regions around an aircraft can be seen in Figure 2.

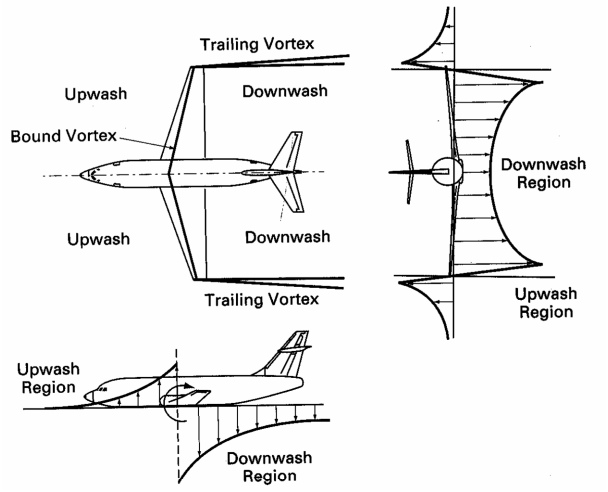

Figure 2. Upwash and Downwash Regions of a General Aircraft (27:46)

There has been considerable time and effort spent in determining the optimal position for an aircraft to receive similar benefits as birds flying in formation. Early research into the profile for maximum drag reduction focused on wing docking, or physically joining the wingman's aircraft to that of the mothership. One such flight test occurred with the docking of an F-84F fighter to a B-36 bomber (22:1,9-10). The flight test concluded with a structural failure of the B-36, resulting in a separation of a 10-foot section of the wing during flight. A detailed analysis of the failure mode revealed an unstable directional, β, aperiodic mode. Research confirmed the existence of the mode that tore the wing during the flight test and revealed a strong pilot induced oscillation potential due to the innate differences in the handling of an aircraft during docked flight.

In a water tunnel analysis of docking flight, it was found that for very small gaps in the spanwise direction, a severe unsteadiness in the flow develops. This unsteadiness was hypothesized to make docking operations very difficult to perform in practice (34:7-

8). Added to this, a wind tunnel analysis of the derived benefits for a dissimilar formation, an F-84 and a B-36, compared the results of three cases; docked formation, towed formation, and close formation (21:16). The results showed the close formation received approximately 27 times the benefit for induced drag as that of the docked formation. The towed aircraft profited on the same order of magnitude as the close formation. Docked formation flight would not only require increased pilot skill but subsequent enhancement to the wingtip structure of the mothership. Additionally, close formation flight has a greater benefit for the trail aircraft. As such, the development of a cooperative formation profile is the focus of this study.

In order to take advantage of the vortices, it is necessary to place the trail aircraft aft of the lead aircraft's wingline, and remain within a range where the vortex has not diminished. This required position resembles "fluid" formation. Fluid formation places the wingman aft of the wingline of the lead aircraft at a range of 1,000 to 3,000 feet (12:3-9, 3-11). The wingman is free to maneuver around the lead to maintain formation, only momentarily passing directly in trail to maintain position. Changes to this basic position would require the trail aircraft to maintain a fixed lateral and longitudinal spacing to gain the benefit of a decrease in induced drag during cruising flight. The effective spacing relative to the lead aircraft would be reduced, with the spacing required resembling "route" formation. Route is defined as 3 feet lateral spacing out to 500 feet, line abreast to slightly aft of lead's wingline.

The illustration in Figure 3 is included to orient the reader with the relative two-ship formation used in this thesis. The left side represents a view of the formation

from above and depicts a set longitudinal spacing, with increasing wingtip overlap being positive. The right side illustrates the vertical separation, where a negative value implies the trail aircraft is at a lower elevation than the lead aircraft. Both the elevation and the wingtip overlap are normalized with respect to the wingspan of the lead aircraft. In this case, the longitudinal spacing, measured from the nose of each aircraft, is set at 200% of the wingspan of the lead aircraft.

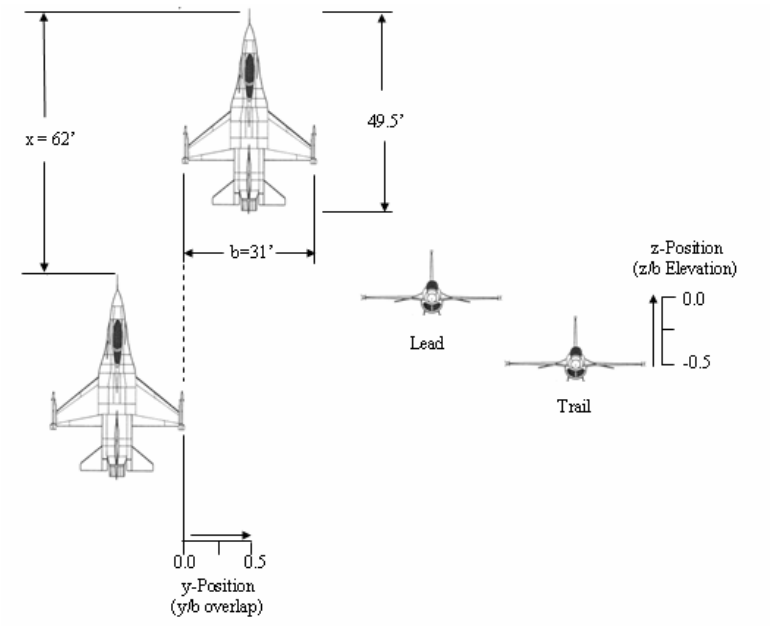

Figure 3. Formation Geometry

The optimal position, in close formation, for a wingman to fly has received considerable attention. Utilizing an approach similar to the analysis of birds in formation, Hummel continued his research into formations of aircraft (19:36-4). The resultant power reduction was identical to Figure 1. Making use of the HVM, Hummel

predicted an optimal wing overlap at approximately 22% wingspan (b). Using a Vortex Lattice Method (VLM) code, Blake and Multhopp predicted the optimal wing overlap to be at 5% wingspan (8:3-6). The horseshoe model used a single vortex to represent the aircraft, while the VLM, further discussed in Chapter 2, represented the aircraft as a finite number of vortices. The difference in the optimal positioning between Hummel and Blake was a result of the method chosen for analysis. Neither of these predictions accounted for flight control trim positions of the trail aircraft. Both the roll and yaw coefficients followed the same general trend, with differing orders of magnitude, as the aircraft was swept along the lateral direction. Assuming the lead aircraft is to the right of the trail, there is a parabolic change in the coefficients going from positive through negative and returning to zero as the aircraft exits the vortex. Hummel's prediction was close to the point of zero rolling moment for the trail aircraft, and Blake's prediction was near the point of maximum negative rolling moment. Wagner noted this discrepancy and applied aileron trim corrections in the roll axis only, arriving at an optimal wingtip overlap of 14% wingspan (35:2-16–2-18).

In attempts to verify the theoretical predictions, several flight tests have been conducted. Hummel used a formation of two Dornier Do-28 aircraft (19:36-2). For the purpose of the flight test, no lateral position inside of zero wingtip spacing was analyzed. Notably, a maximum power reduction of 15% was observed at the minimum spacing. Wagner conducted a flight test using two United States Air Force (USAF) T-38 aircraft at 10,000 feet and 300 Knots Indicated Airspeed (KIAS) (35:4-5). A series of tests were conducted incorporating a lateral sweep of the trail aircraft to test the theoretical HVM,

un-trimmed VLM, trimmed VLM, and zero-overlap positions. The optimal position was determined to be the predicted trimmed VLM 14% overlap, with a realized drag savings of 8.8 ± 5%. However, the analytical prediction for drag savings was 15% (35:2-18). The flight test used visual references to maintain formation position (35:4-1). Pilots were able to assess changes in relative position while flying in the vortex position, but were unable to determine their actual spacing. Additionally, the test did not investigate changes in vertical positioning.

The final flight test of note was that of the National Aeronautics and Space Administration (NASA) (33:8-9, 17-25). During the test of two F-18A aircraft at 26,000 feet and 300 KIAS, varying positions of the trail aircraft were observed. The trail aircraft was moved in three dimensions during the test, with the optimal drag reduction of 20% occurring at 150% longitudinal spacing, -6% vertical spacing, and 13% wingtip overlap. These coordinates are in the percentage of the wingspan and referenced off the nose of the trail aircraft. In the assessment of the flight test, it was observed that a wingtip overlap more than 30% resulted in a highly unstable region, and positions with no wingtip overlap were considerably more controllable.

Verified through both numerical analyses and flight test results, there exists a region for aircraft in formation to achieve a considerable benefit from close formation flight. Basic theory from birds to aircraft is nearly identical; however, there are discrepancies in where the position of the trail aircraft should fly and the actual realized benefits that could be gained by this profile. A limited numerical analysis, focusing on implementing only aileron trim, has been conducted moving the optimal overlap from 5%

to 14% for a similar formation (35). This has been correlated through two subsequent flight tests, however the derived savings for both tests varies by a factor of 2, 8.8% versus 20%. Additionally, during the wind tunnel analysis of a dissimilar profile, the predicted induced drag savings by flying in close formation was nearly 1100% over that of free flight (21:1), a relatively large benefit worthy of further numerical evaluation.

Scope of Research

The purpose of this research is to quantify the position of greatest drag reduction in the two-ship formation profile. This will be accomplished using a computational analysis based on the VLM. The capacity of the computational code has expanded since the work of Wagner, and the fidelity of the model will be increased. Additionally, the analysis will incorporate trimmed flight control predictions in two axes: roll and yaw. The introduction of both trim axes is expected to provide additional insight into the predicted lateral spacing of the trail aircraft. Previous research focused on cruise airspeed, approximately 300 KIAS, as the test point. Airspeed is frequently changed to meet the needs of specific aircraft requirements as well as those of air traffic control; therefore, an analysis of the various airspeeds associated with general formation profiles will be completed to determine potential changes in position as well as expected overall drag reduction. Incorporated into the flight test profile will be a variation in the vertical separation of the trail aircraft. This will be an attempt to validate the VLM predictions with the real observations made during NASA's flight test. Finally, a dissimilar

formation profile of a tanker aircraft and a fighter size aircraft will be investigated to explore the benefits of a cruising profile often encountered in military aviation. This investigation will include changes in the vertical spacing of the trail aircraft as well as trimmed flight control positions about the same axes as the similar formation.

Limitations of Research

The major limitations in the context of this analysis will be during the flight test phase. The measured fuel flow reading of the flight test instrumentation system is calibrated to match the cockpit gauge and takes the reading from a production fuel flow meter, with a resolution of ±20 pounds per hour and an uncertainty of ±100 pounds per hour. The resultant uncertainty in the calculation of the difference in fuel flows is 200 pounds per hour. For the flight conditions for the test, this corresponds to a resolution of ±7 percent in the fuel savings calculations. To minimize the impact of this error source, data from flight-test instrumentation for the engine speed and airspeed changes were collected to correlate relative fuel savings of the formation. The core engine speed has a resolution of ±0.01 percent, and the calibrated airspeed has a resolution of ±0.07 knots.

The digital electronic engine control of the F-16 F100-PW-220 engine continually adjusts fuel flow and rpm to optimize engine operation (13:1-56). In the primary operating mode of the engine, the engine control schedules fuel flow, in addition to controlling nozzle position, compressor inlet variable vanes, and rear compressor inlet variable vanes. During the flight test, these changes in engine operating parameters were

most apparent in the 10 seconds following a power lever angle adjustment. As such, stable engine parameters were difficult to achieve, as power corrections were typically required before the engine had sufficient time to trim to optimum conditions. These variations in engine parameters not only affected the analyses of both the airspeed and engine speed methods but also increased the pilot workload to maintain position.

The positions flown during the flight test were determined following the mission through a differential Global Positioning System (GPS) solution. No capability exists to display the relative displacement to the pilot in real-time and post processing was used. To minimize this limitation, an assessment of the relative position of the lead aircraft was made on the ground. Using the assessment, suitable visual references were determined to assist in maintaining the proper displacement from the lead aircraft. The actual position flown was calculated post-flight.

Minor limitations exist within numerical analysis of formation flight. As with any model, attention to aircraft geometry is paramount. However, the incorporation of two computational models within the predictive code requires modifications to the basic geometry. The lateral spacing of the overlapping regions of the aircraft must align. This will be discussed in greater detail in Chapter 2. As such, adjustments to the basic lateral geometry of the models to allow for a computational stable analysis of the aircraft need to be made.

Finally, the VLM does not account for any change in altitude of the vortices. As such, the numerical analysis of the similar formation will not account for any changes in elevation of the trail aircraft. The associated change in elevation will be investigated

during the flight test phase. NASA's test revealed a 6% span drop in the vortex for a 150% longitudinal spacing. This study shall focus on a region at 200% span longitudinal spacing and provide insight into the relative shift of the trailing vortices during the optimal formation profile.

Payoff of Research

With the investigation into an optimal drag reduction close formation flight profile and the incorporation of a station-keeping autopilot, the range of a formation of aircraft can be considerably increased. A trail aircraft in a formation need only fly in the best position in the vortex generated by a lead aircraft. There are no modifications to existing hardware required; no engine overhauls, no structural modifications, and best of all, no paper to production new aircraft designs. The only cost associated would be the incorporation of a software modification of the autopilot to completely realize the true benefit. Overall, this is a free benefit from the principles of aircraft in flight. Fighter-type aircraft would apply a similar formation profile in an emergency fuel situation. Likewise for a dissimilar formation, such as the ubiquitous tanker-UAV profile, a flight in this profile would either reduce the number of autonomous refuelings required, or increase the overall distance that the formation could travel. The benefits are applicable to both the military and the civil aviation communities.

Thesis Outline

The remainder of this thesis will focus on a 2-ship formation. Background will be provided into the application of Munk's Stagger Theorem to the study of close formation flight. The utilization of the VLM in an aircraft analysis will be discussed. Following, a description of the computational code will be presented.

An analytical analysis of two distinct formation profiles will be discussed. The first formation will be an F-16B and an NF-16D aircraft, a similar formation. This examination will incorporate the effects of trimming the aircraft in roll and yaw, as well as varying the velocity of the formation. The second study will focus on a dissimilar formation consisting of a lead KC-135R aircraft and trail NF-16D aircraft. This will look at the effects of changes in the altitude of the trail aircraft using the predictive code, and will incorporate the same trim actuations.

The final portion of the study will focus on flight test with a similar formation profile to include a detailed analysis of the flight test set-up and follow through with the flight test results. The flight test will allow a comparison of the predicted drag benefits from the VLM analysis to the realized flight test results.

II. 2-Ship Analytical Background

Chapter Overview

Prior to the analysis of the drag reduction expected from a formation aircraft, a conceptual analysis of a 2-ship formation will be discussed. In it, the basic concept of how an aircraft flying in the vortices of another aircraft experiences an associated drag reduction will be examined. The groundwork will then be laid to successfully analyze the formation according to modern theory. Finally, the computational program that will be utilized is explored. A discussion in the basic theory of the computer code will be presented prior to the information regarding this specific system.

Trail Aircraft Analysis

A trail aircraft flying in the upwash region generated by the lead aircraft experiences a shift in the relative angle of attack, as compared to solo flight, reference Figure 4. The subscript "f" denotes the aircraft flying in formation.

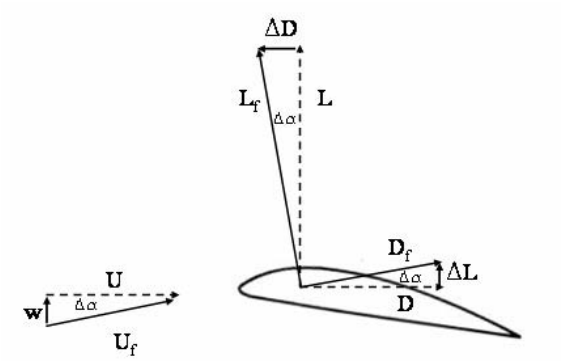

Figure 4. Change in Relative Angle of Attack (19:36-2)

Several assumptions are necessary for this basic analysis. First, there is a negligible change in the free-stream velocity; $U \approx U_f$ and U>>w, the upwash velocity. Second, at normal cruise conditions, the magnitude of lift, L, is much greater than the magnitude of drag, D; L >> D. Furthermore, by making use of a small angle approximation,

$$\Delta\alpha = \tan\left(\frac{w}{U}\right) \approx \frac{w}{U} \tag{1}$$

Application of these assumptions and approximations to the situation depicted in Figure 3 yields:

$$L = L_f \cos(\Delta\alpha) + D_f \sin(\Delta\alpha) \approx L_f + D_f \Delta\alpha \approx L_f + D_f \frac{w}{U} \approx L_f \tag{2}$$

$$D = D_f \cos(\Delta\alpha) - L_f \sin(\Delta\alpha) \approx D_f - L_f \Delta\alpha \approx D_f - L_f \frac{w}{U} \tag{3}$$

Or the difference in drag can be expressed as:

$$\Delta D \approx -L_f \frac{w}{U} \approx -L \frac{w}{U}$$

For an aircraft properly positioned in the upwash region of lead's aircraft, there is a slight change in the lift, but, more importantly, a significant reduction in drag. From a pilot's perspective, the change in lift, even though assumed negligible in the mathematical analysis, will result in a minor reduction in the pitch attitude to maintain vertical position. Likewise, the decrease in drag will result in a power reduction to preserve proper longitudinal spacing. Over time, the net result on the trail aircraft from the reduction in drag will be a decrease in fuel consumption.

The approach used to analyze the 2-ship formation drag reduction was based upon Munk's Stagger Theorem (26:375). As the theory states, the relative change in induced drag is dependent upon the geometry and size of the formation. This deals with the entire system of aircraft. As the longitudinal, or downstream, spacing increases, the trail aircraft receives nearly all the benefit for the formation. Expanding upon Munk's work, Prandtl developed a method to analyze biplane and triplane designs of aircraft (28). The topic of multiplane research has been in existence since the 1920s. Prandtl's method determines the induced drag for each lifting body as:

$$C_{D,k} = C_{D,k_0} + \sum_{k \neq j} K_{kj} C_{L,k} C_{L,j} \tag{4}$$

In Equation 4, the subscript "0" represents the aircraft flying in solo flight. This method allows for different lift coefficients to be flying in formation. Applying Equation 4 to a system of two aircraft results in the following relationship for the trail aircraft:

$$C_{D,2} = C_{D,2_0} + K_{12} C_{L,1} C_{L,2} = K_0 C_{L,2}{}^2 + K_{12} C_{L,1} C_{L,2} \tag{5}$$

The variable K_{12} represents the relation between the various aircraft in a formation. Upon further investigation of equation 5, the sign of K_{12} must be negative for a reduction in the induced drag to occur. If K_{12} is positive, there will be an increase in the induced drag of the system, and it can be implied that the aircraft is flying in the downwash region, thus not experiencing any benefit. Solving for K_{12} yields:

$$K_{12} = \frac{C_{D,2} - K_0 C_{L,2}^{\ 2}}{C_{L,1} C_{L,2}} \tag{6}$$

K_0 is obtained from the drag polar of the aircraft operating independently of the formation. Therefore, the ratio of K_{12} to K_0 is the applicable percentage reduction in the induced drag. The induced drag reduction ratio will be defined as R, where:

$$R = \frac{K_{12}}{K_0} \tag{7}$$

To this point, the only component of drag to have been discussed is induced drag, $C_{D,i}$. However, the total drag of a body in flight is the summation of the parasite and induced drag.

$$C_D = C_{D,0} + C_{D,i} \tag{8}$$

By flying in a drag reduction profile, the induced drag on the aircraft will be reduced by the percentage, R. The net change in drag for the trail aircraft in the system is:

$$C_{D,f} = C_{D,0} + (1 - R) C_{D,i} \tag{9}$$

The reduction in total drag of the system can then be expressed as a ratio of the formation drag, $C_{D,f}$ to the single aircraft in flight drag, C_D. For an aircraft properly situated in the upwash region, the ratio is less than 1, i.e.:

$$\frac{C_{D,f}}{C_D} < 1 \tag{10}$$

As a measure of performance, the reduction in drag has a direct correlation to power savings. From an analysis of an aircraft in straight and level flight (4:264), where weight equals lift and thrust equals drag, the thrust required can be expressed as:

$$T_R = W\frac{D}{L} = W\frac{C_D}{C_L} \tag{11}$$

Additionally, the power required is the thrust required multiplied by the freestream velocity:

$$P_R = T_R U = WU\frac{C_D}{C_L} \tag{12}$$

From this analysis, it is clear to see that a percentage reduction in drag will produce the same relative power savings for the aircraft. This theoretical reduction in drag of the formation corresponds to a decrease in fuel flow for an aircraft.

Munk's Stagger Theorem states that the induced drag of a system is dependent upon the number of entities and the shape of the formation. For the purpose of this analysis, the number of elements in the formation is kept constant at two, and the only variation will be in the shape of the formation. The previous work of Wagner determined that increasing the size of the formation would achieve greater benefits for additional trailing aircraft (35:2-22). In this research, the shape of the formation will be adjusted by

changing the lateral spacing of the formation in incremental steps. At each increment, the necessary values of the variables in Equation 6 need to be ascertained. Also, a computational analysis of a solo aircraft operating at the same conditions as the formation needs to be performed to determine the remaining variables.

Vortex Lattice Method

A fundamental method for analyzing the mechanics of a formation of aircraft has been the VLM. Traditionally, the VLM has been useful in the study of subsonic airflow over airfoils and aircraft structures. The theory utilizes two concepts during the aerodynamic analysis; simplifying the structure into finite number of horseshoe vortices of circulation strength (Γ), and applying these horseshoe vortices and their interactions to each element of a mesh comprising the structure (3:391-398, 6:260-278).

The horseshoe vortex acting on each elemental component, Figure 5, consists of three separate pieces, two unbounded vortices extending to infinity in the longitudinal direction, components $\overrightarrow{ba}$ and $\overrightarrow{cd}$, and one bounded vortex, $\overrightarrow{bc}$, situated on the quarter chord line, $l/4$, oriented in the spanwise direction of each element. Each element contains a control point that is situated mid-span at the $3/4l$ in the longitudinal direction.

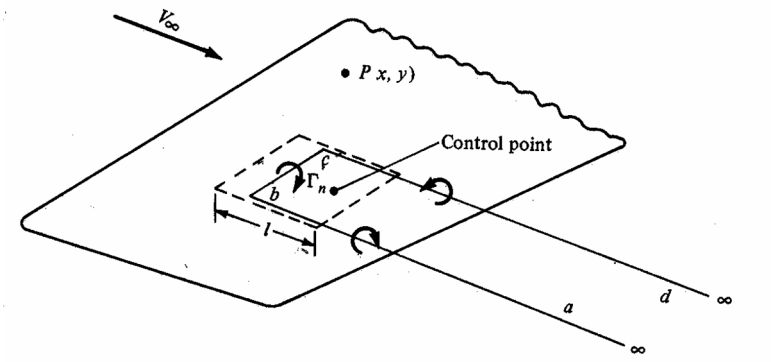

Figure 5. Elemental Horseshoe Vortex (3:395)

Making use of the Biot-Savart Law, Equation 13, individual perturbation velocities at specified control points can be calculated based on the interactions between the vortex elements.

$$d\vec{v} = \frac{\Gamma_n}{4\pi} \frac{d\vec{l} \times \vec{r}}{\left|\vec{r}\right|^3} \tag{13}$$

where $d\vec{l}$ is the *incremental length* of the vortex filament for integration, and $\vec{r}$ is the *positional vector* from the incremental vortex filament length to the control point.

To gain an insight into the application of Equation 13, the case of a planar wing will be discussed. For this case, Bertin (6:268) expands Equation 13 to:

$$
\begin{aligned}
w_{m,n} = \frac{\Gamma_n}{4\pi}\Bigg\{ & \frac{1}{(x_m - x_{1n})(y_m - y_{2n}) - (x_m - x_{2n})(y_m - y_{1n})} \\
& \Bigg[\frac{(x_{2n} - x_{1n})(x_m - x_{1n}) + (y_{2n} - y_{1n})(y_m - y_{2n})}{\sqrt{(x_m - x_{1n})^2 + (y_m - y_{1n})^2}} \\
& - \frac{(x_{2n} - x_{1n})(x_m - x_{2n}) + (y_{2n} - y_{1n})(y_m - y_{2n})}{\sqrt{(x_m - x_{2n})^2 + (y_m - y_{2n})^2}} \Bigg] \\
& + \frac{1.0}{y_{1n} - y_m}\left[1.0 + \frac{x_m - x_{1n}}{\sqrt{(x_m - x_{1n})^2 + (y_m - y_{1n})^2}} \right] \\
& - \frac{1.0}{y_{2n} - y_m}\left[1.0 + \frac{x_m - x_{2n}}{\sqrt{(x_m - x_{2n})^2 + (y_m - y_{2n})^2}} \right] \Bigg\}
\end{aligned}
\qquad (14)
$$

In Equation 14, "m" denotes the panel being analyzed and "n" is the panel whose vortex is affecting the control point of the m^{th} panel. The position (x_m,y_m) represents the coordinates of the control point under assessment. The positions (x_{1n},y_{1n}) and (x_{2n},y_{2n}) are the coordinates of the left and right portion of the bound vortex, respectively. A lattice of a structure would reduce to an algebraic, albeit complex, system of resulting equations. The solution to the system requires the flow be subject to the boundary condition of no flow through the surface.

Finally, the resulting induced upwash velocity at the control point can be calculated via a summation of the individual resultant velocities determined from Equation 14.

$$w_m = \sum_{n=1}^{N} w_{m,n} \tag{15}$$

N is the total number of elements for the structure. At this juncture, the individual bound vortex strengths, Γ_n, can be determined through the application of the boundary conditions.

To determine the resulting lift and induced drag coefficients of the structure, the mathematical integration is transformed into a summation of the discretized elements. The free-stream velocity and density are assumed constant.

$$C_L = \frac{1}{q_\infty S} \int_{-b/2}^{b/2} \rho_\infty U_\infty \Gamma(y) dy = \frac{2}{U_\infty S} \sum_{n=1}^{N} \Gamma_n \Delta y_n \tag{16}$$

$$C_{D,i} = \frac{1}{q_\infty S} \int_{-b/2}^{b/2} \rho_\infty U_\infty \Gamma(y) \alpha(y) dy = \frac{2}{U_\infty S} \sum_{n=1}^{N} \Gamma_n \alpha(n) \Delta y_n \tag{17}$$

Having determined the forces acting on the aircraft, resulting moments, yaw and roll, can be determined having a known center of gravity (c.g.) reference point. For a truly symmetric aircraft, these coefficients will be approximately zero for a planar wing analysis.

Extending this analysis to a system of aircraft, the number of elemental components is pre-determined for each structure. The perturbation calculations for the elemental interactions are based on the geometry and, although the number of calculations is increased, the method remains the same. Let N be the total number of

panels for the lead aircraft, and M represent the elements of the trail aircraft. The individual affects of the vortex interaction, Equation 15, would need to incorporate all components of the system. Thus the limits of the summation would extend to N+M components. The summation limits for Equation 16 and 17 would remain the same for the lead aircraft. However, the trail plane limits would be from N+1 to N+M. In the case of completely similar aircraft in formation, M is equal to N.

To gain an understanding of the methodology of the VLM, the basic concepts have been discussed. The program utilized in this analysis is a NASA-developed FORTRAN-based code incorporating the VLM techniques (1). The specifics of the program will be discussed in the next section.

HASC95

NASA developed the High Angle of Attack Stability and Control code, HASC95, for deeper investigation into a new analytical/semi-empirical aerodynamic prediction method (1). The code incorporates three routines: a generalized vortex lattice program, a semi-empirical strake vortex analysis code, and a 2-dimensional, unsteady, separated flow analogy program. The program uses a flat-wake approximation in the representation of the trailing vortices. This approximation extends the trailing vortices to infinity in the x-y plane. HASC95 utilizes this predictive method to obtain the flight coefficients on the structure. The specifics of the program are outlined in the user's manual. The operating procedures are outlined in their application to this study. In analyzing a single-ship configuration, the basic HASC95 code will be used.

The input file is the geometry of the structure to be analyzed. The body is reduced to a series of finite points that outline the structure. Each individual component is termed as a panel. A series of panels comprise a surface, such as a wing. Finally, the combination of surfaces determines the structure. Internal to each panel, the number of divisions within each is defined. These divisions occur in the spanwise and chordwise directions. A description is shown in Figure 6. Additionally, the input file used in the analysis of this report is contained in Appendix B.

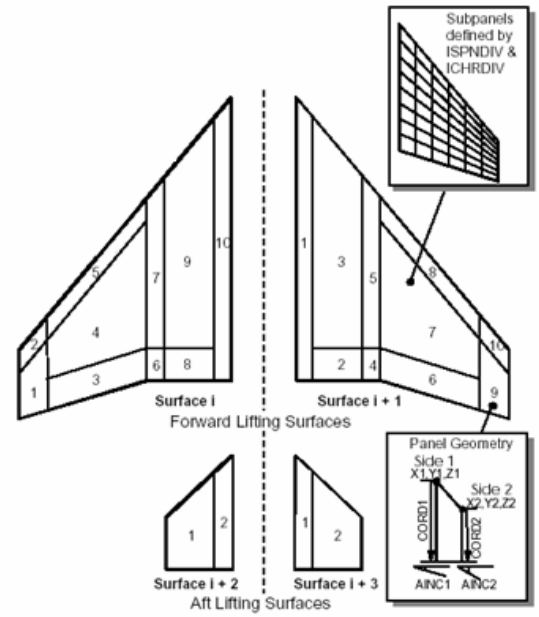

Figure 6. HASC95 Geometry Description (1:53)

The predictive code outputs the following aerodynamic coefficients; lift, drag, pitch, side force, roll, and yaw. To account for flight control trim positions, each control surface is modeled as a separate panel. This allows for the introduction of an incidence

angle to that surface, simulating a trim condition. For the purpose of this analysis, the roll and yaw coefficients, C_l and C_n, were the orders of merit. Thus driving these to zero would imply a trimmed aircraft in those axes.

The analysis in this research is not limited to a single aircraft, and the code is ambivalent to the actual geometry of either structure. To gain useful information, the geometry of the lead aircraft's lattice must align with that of the trail aircraft in the overlapping regions, as shown in Figure 7. This is a limitation of the computer code and prevents the unbound vortices from aligning with the control points of the trail aircraft and creating a computationally unstable alignment.

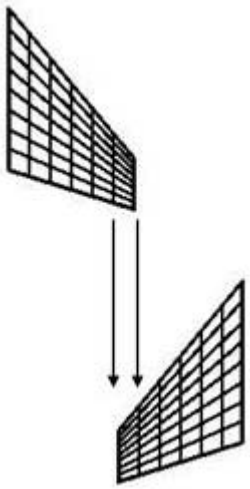

Figure 7. Lead-Trail Vortex Alignment

To accomplish the more-involved formation analysis, Mr. Blake, Air Force Research Laboratory (AFRL), created a modification code (7). The modification involved two additional subroutines in addition to the basic code. Both subroutines are

provided in Appendix D. The first subroutine, mice.f, allows for the computational movement of the lead aircraft in the formation, and thus varying the lateral spacing of the formation. The lead aircraft is swept across in a desired dimension for analysis. For this analysis, the longitudinal and vertical spacings were predetermined for a given scenario, and the position of the lead aircraft was varied in the y-dimension, or lateral axis. Changes in the elevation, during the dissimilar formation analysis, were manually entered into this subroutine. The second subroutine, printemp.f, is a modified subroutine that extracts the desired coefficients of each structure in the simulation, at the given incremental changes in the lead aircraft position determined by the HASC Modifications, and outputs those results to a designated file.

As a result of varying the lateral position of the lead aircraft, multiple stations of the aircraft will overlap during the analysis at any given step. As previously discussed, the HASC95 program required the trailing vortices to align for a stable solution. To accommodate the geometrical requirements, the span-wise elemental breakdown was chosen to be consistent within the formation. As a result, minor modifications to the aircraft geometry were implemented.

The following chapter will review the analysis of two formation profiles. The process will proceed with the model production and validation. A 2-ship analysis will be conducted on a similar aircraft profile operating at realistic conditions. The specifics of the flight control trim position actuations will be presented in the context of a similar formation. The chapter will conclude with the analysis of a dissimilar formation profile, capturing the same elements as the similar formation examination.

III. Analytic Analysis

Chapter Overview

This chapter will continue with the specific analysis of the desired formations. First, the model production will be detailed, followed by a discussion of the desired test points. The importance of a quality computational model is paramount, and the structure will be compared to wind tunnel data. The following analysis of the formation profile will be divided into two specific divisions: a focus on a similar formation incorporating variations in airspeed and flight control trim actuations and a dissimilar formation investigating various altitude positions as well as the same trim actuations as the similar profile.

Model Production

For the purposes of these analyses, a Lockheed Martin NF-16D Variable stability In-flight Simulator Test Aircraft (VISTA) will be used as the trail aircraft platform in the formation studies. For the corresponding lead aircraft in the similar formation study, an F-16B will be used. These aircraft were chosen based on the expected flight test platform for data collection. The dissimilar formation lead aircraft will incorporate a Boeing KC-135R Stratotanker. This was selected based on the relevance of a formation of

UAVs flying in extended cruise with the tanker. The VISTA will remain the trail aircraft to provide useful information for future manned-flight testing of the profile.

In developing the model, existing aircraft schematics (30:4) were analyzed with slight modifications to the aircraft necessary to interact with the HASC95 code. These variations were necessary in the model to allow the modified HASC program to vary the lateral position during the simulation, as previously discussed. Aircraft dimensions are shown in Appendix A, with the developed model shown in Figures 8 and 9. Additionally, the VISTA input data file for the HASC95 program is in Appendix B. All dimensions for the computational model are in inches. A discussion of the modified dimensions follows.

Notably, the code does not allow for a "true" three-dimensional modeling of the structure. Essentially, the aircraft was modeled as two perpendicular 2-dimensional planes intersecting at the aircraft centerline, a wing plane and a vertical plane. This representation allowed primarily for the aerodynamic effects imparted on the vertical tail to be accounted for in the later trim analysis. Additionally, the strakes of the F-16 possessed some lifting characteristics, and care was taken to accurately represent the structure. Furthermore, the wingline was chosen as the reference plane, and the nose was assumed to be in a straight line with the tail of the aircraft. The final significant modeling assumption was the placement of the ventral fins. The fins on the actual aircraft are positioned on the underside of the engine nacelle, providing for adequate directional stability characteristics. For the purpose of the simulation and the integration into the

HASC95 code, the z-position of the ventral fins was altered to be in line with the wing plane. Their position in the longitudinal dimension remained unaltered.

Minor modifications exist in the lateral dimension of the model. In conducting a sweep of the aircraft in the lateral dimension, a discretized step size needs to be accounted for in determining the lateral dimension spacing of the elements, and subsequently, the lateral panel alignment of the computational model between the lead and trail aircraft representations. The chosen incremental step was 5 inches, and the lateral dimension of both F-16 aircraft was tailored to meet this constraint. The actual aircraft wingspan is 372 inches, whereas the computer model is 370 inches. The net difference of approximately 0.5% in the wingspan is considered to be insignificant. A representation of the model in the x-y and x-z plane can be seen in the following Figures 8 and 9.

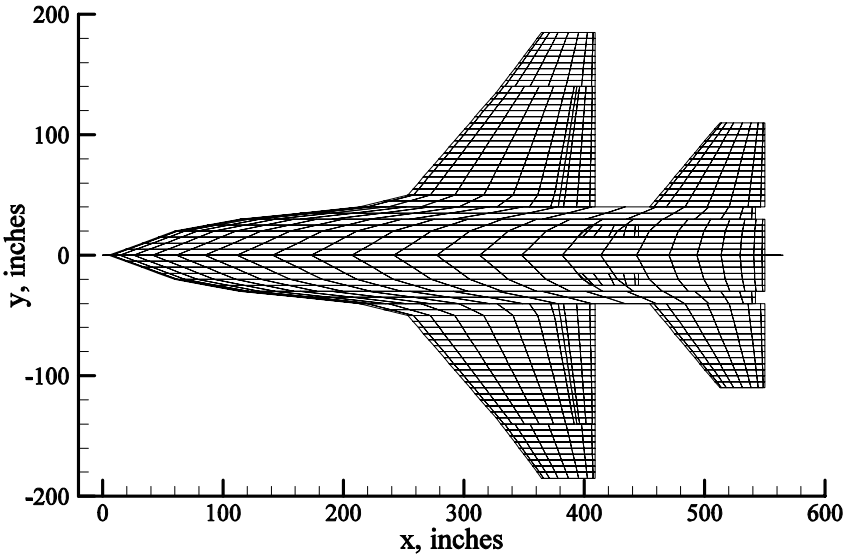

Figure 8. NF-16D VISTA, Computational Mesh, Top View

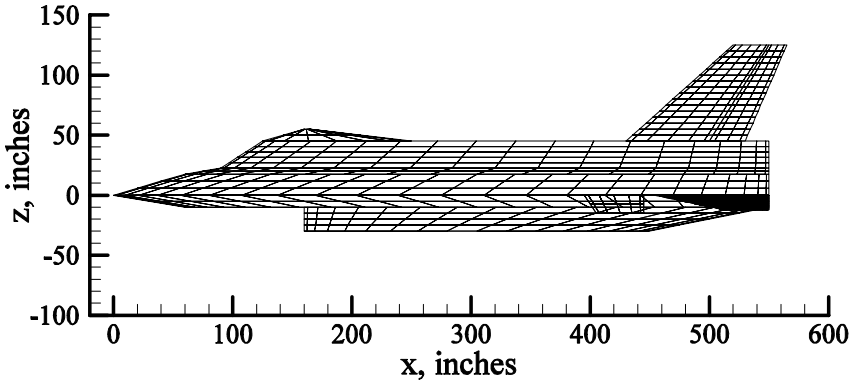

Figure 9. NF-16D VISTA, Computational Mesh, Side View

The VISTA was modeled as a structure consisting of 26 panels; 16 in the wing plane and 10 in the vertical plane. For the x-y plane, Figure 8, the following 8 panels existed, symmetric for the left and right side of the aircraft: 1. Nose Section, 2. Speedbrake Section Forward, 3. Forebody, 4. Inboard Wing Strake, 5. Forward Wing, 6. Flaperon, 7. Wing Tip, and 8. Horizontal Stabilator. The x-z plane consisted of 10 panels, Figure 9: 1. Upper Nose, 2. Lower Canopy, 3. Mid-Canopy, 4. Upper Canopy, 5. Vertical Tail, 6. Rudder, 7. Lower Nose, 8. Engine Nacelle, 9. Left Ventral Fin, and 10. Right Ventral Fin.

The first simulation was chosen to be representative of the anticipated flight test profile. The VISTA schematics were compared to the F-16B (37:1-9), shown in Appendix A. The aircraft are similar, but minor differences exist. Noticeably, the horizontal stabilator is reduced in size, and the aircraft spine is lower than that of the VISTA. All other dimensions remain the same. These 2 modifications were made to the design of the F-16B model. The HASC95 data files for the F-16B and the NF-16D are

included in Appendix B. Despite the minor differences in geometry, this formation was considered to be similar for this analyis.

The KC-135R Stratotanker model used in the dissimilar study was previously developed by AFRL. A technical drawing was reviewed to ensure the validity of the representation (10). This is shown in Appendix A. The fuselage of the tanker was not designed as a primary lifting surface, and was considered unnecessary in the building process, as with the F-16. Additionally, the assumed optimal position for the tanker profile placed the trail aircraft outboard of the number one or number 4 outboard engines, wing station 545, measured in inches. This was to avoid the engine exhaust. Therefore, the working KC-135R model was determined to be adequate for this analysis. The paneling in the lateral dimension was altered to be 15 inches. This allowed for a computationally stable analysis with the unbound vortices of the lead aircraft aligning with those of the trail aircraft. In determining the position of the alignment of the horizontal tail, a gross weight of 215,000 pounds and c.g. position of 25% mean aerodynamic chord were assumed. The KC-135R's trim system for the horizontal tail moved the entire surface, and performance specifications (17) were reviewed to determine a horizontal tail setting of –5.7° for the assumed flight conditions.

Test Point Selection

To subsequently determine the drag reduction benefits, test points were determined. For this simulation, an altitude of 20,000 feet was used for all cases. This altitude will begin to represent a cruising profile for extended flight. Standard atmospheric data was used with density of $0.001266\,\text{slugs}/\text{ft}^3$ and viscosity of $3.324 \times 10^{-7}\ \text{lb}_f\text{s}/\text{ft}^2$. These were used in the determination of the Reynolds number, required in the HASC input data file. Additionally, three test airspeeds were chosen. These were determined for an aircraft gross weight of 24,000 pounds with a c.g. location of 320 inches aft of the nose. The first airspeed selected was 300 KIAS, generalized tanker cruise airspeed, chosen for simulation of aircraft in trail of a tanker during an ocean crossing or ferry flight scenario. This was the only airspeed considered during the dissimilar profile. The next two airspeeds were chosen to simulate an F-16 in a fuel-limited scenario: maximum range airspeed of 271 KIAS and maximum endurance airspeed of 211 KIAS. The F-16 performance manual was used to determine the airspeeds for these conditions (14:C4-33). Table 1 summarizes the three test cases.

Table 1. Test Data Cases

Test Case	Velocity Type	V_{true} (kts)	Mach Number	$V_{calibrated}$ (kts)	$V_{indicated}$ (kts)	V_{true} (ft/s)
1	Tanker Cruise	401	0.65	301.00	300.00	668.33
2	Max Endurance	291	0.47	212.00	211.00	485.00
3	Max Range	366	0.60	272.00	271.00	610.00

Assuming straight and level flight at 20,000 feet and these tabulated values of airspeed and gross weight, the necessary lift coefficients were determined by:

$$C_L = \frac{W}{\frac{1}{2}\rho U^2 S} \tag{18}$$

Based on the determined test configurations, the computational approach was the matching of the desired lift coefficients to those obtained during the HASC95 simulation. Utilizing this approach, the angle of attack for the HASC95 program was iterated upon. The following is a list of the predicted lift coefficient value, the final iterated HASC95 value, and the resultant angle of attack, α.

Table 2. HASC95 Input Data

Test Case	V_{true} (ft/s)	C_L (desired)	C_L (HASC)	HASC α (degrees)
1	668.33	0.2592806	0.2592	3.67
2	485.00	0.4923487	0.4919	7.32
3	610.00	0.3112409	0.3110	4.47

Not shown in this table is the dissimilar profile angle of attack. As this is based upon the lead aircraft, the KC-135R model was determined to need an α of 2.99° to maintain level flight. Having determined the operating conditions of the simulation, it is necessary to accurately relate the computational data into actual induced drag savings. A baseline comparison of a solo NF-16D aircraft operating at the same flight was performed. Specifically, the single ship drag and lift coefficients were needed to relate the validity of the model to that of wind tunnel data.

Test Model Validation

Validation of the model was accomplished at a Mach of 0.2 and α ranging from 0° to 10°, with a correlation being made in the numbers of merit: induced drag coefficient, $C_{D,i}$, and lift coefficient, C_L. Data from the HASC95 simulation was compared to wind tunnel data for the VISTA (29:61, 27:A-43). Wind tunnel data was collected at NASA Langley Research Center on a 0.15 scale model in the 30x60 foot wind tunnel. The selected airspeed was representative of the test conditions for the collected data. Subsequent runs were made at higher airspeeds, to capture the expected test profile, with no significant change in the resultant data. Through direct data comparison to the wind tunnel data, a $C_{D,o}$ value was determined to be 0.02. Figure 10 represents a comparison between the drag polars of the wind tunnel data and the HASC95 model.

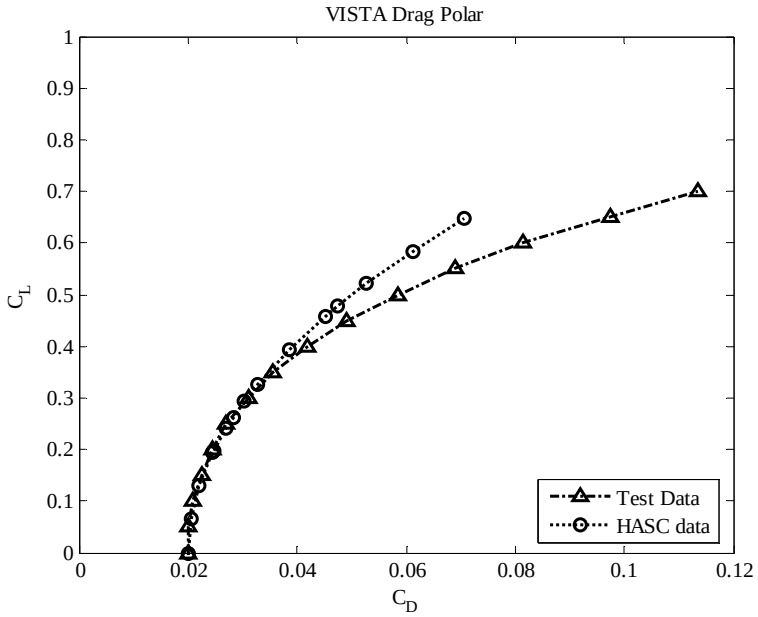

Figure 10. Drag Polar Comparison

As seen from Figure 10, for low lift coefficients, corresponding to $\alpha < 5^{\circ}$, the developed model truly represents the lift and drag relations of the VISTA airframe. For the four test cases, it was determined that the HASC95 model generated a valid solution for comparison, by using the C_L matching technique described previously. Table 3 depicts the variation in C_D from the test data.

Table 3. HASC95 Test Point Validation by Comparison to Wind Tunnel Data

Test Case	α (degrees)	C_L (HASC)	C_D (HASC)	C_D (Test)	Percent Difference
Similar 300 KIAS	3.67	0.25	0.027	0.0265	1.81
Similar Max Range	4.47	0.2925	0.0303	0.0304	-0.3814
Similar Max Endurance	7.32	0.4771	0.0475	0.0541	-12.2791
Dissimilar 300 KIAS	2.99	0.1959	0.0246	0.0243	1.0848

Additionally, the model's yaw coefficient, C_n, and roll coefficient, C_l, values were mathematically zero for all configurations. This corresponds to the wind tunnel testing (31:A-43). The maximum endurance airspeed has the highest difference. However, the focus of the investigation is to prove a relative drag savings benefit. As a result, the VISTA computational model was considered representative for analysis.

To conduct an analysis of the power savings benefit, the aircraft parameters while operating as a single entity needed to be determined. HASC95 was subsequently run at the operating airspeeds, and the baseline single-ship configuration data, shown in Table 4, were ascertained.

Table 4. Single-Ship Operating Conditions

Test Case	α (degrees)	C_L	$C_{D,i}$	$C_{D,o}$	C_D
Similar 300 KIAS	3.67	0.2592	0.0078	0.02	0.0278
Similar Max Range	4.47	0.3110	0.0113	0.02	0.0313
Similar Max Endurance	7.32	0.4919	0.0287	0.02	0.0487
Dissimilar 300 KIAS	2.99	0.2111	0.0053	0.02	0.0253

F-16B and NF-16D VISTA Similar Formation, Analytic Solution

For the purposes of the analysis, as well as safety requirements during the flight test stage, the longitudinal position for the F-16B and VISTA aircraft was set at 62 feet. This provides for a nose to tail separation of approximately 12 feet. At this spacing, the trailing edge vortex will not have begun to break down, as the predictive VLM nature of the code extends the unbounded vortices infinitely in the downstream direction. This

longitudinal position was also similar to the spacing flown by Wagner in the T-38 analysis. For safety of flight considerations, the aircraft will be in a position to recover should a major flight path deviation occur, precluding inadvertent aircraft collision. The trail aircraft's position in the z-dimension was chosen to be with the nose of the trail aircraft aligned with the wing line of the lead aircraft. Due to the lack of dihedral or anhedral in the F-16B's wing geometry, and HASC95's trailing vortex alignment extending to infinity in the x-y plane, no analytic study was accomplished for aircraft located out of plane in the z-direction. Finally, the lateral position was varied from y/b of 0 to 1.4, with incremental changes of 5 inches. A lateral spacing of 1.4 provided a 40% wingtip separation, or 150 inches. A spacing of 0 aligned the trail aircraft directly behind the lead aircraft in line with the engine exhaust, assumed not to be the ideal position. A point worth mentioning is that the span in the lateral spacing ratio is normalized based upon the lead aircraft. This analysis in the y-dimension provided the optimal location to fly to achieve the highest induced drag reduction for the trail aircraft in formation. A depiction of the analytic formation is shown in Figure 11.

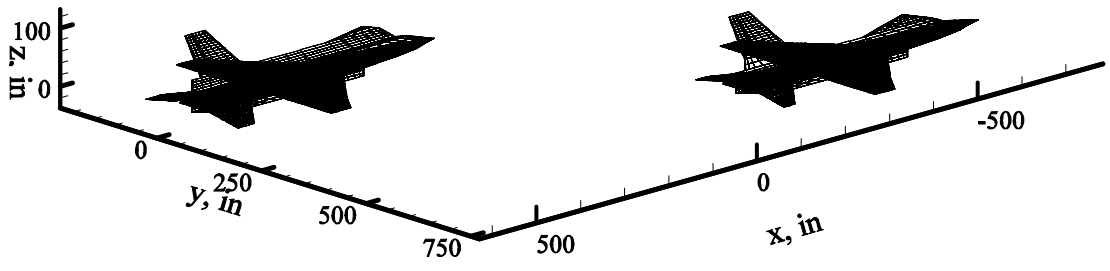

Figure 11. F-16B and NF-16D VISTA Formation

With no introduction of trim surface deflection, Figures 12 and 13 represent the induced drag savings and the roll and yaw moments on the trail aircraft as the position was changed in the lateral dimension. The calculations performed in this study are those previously introduced in Chapter 2.

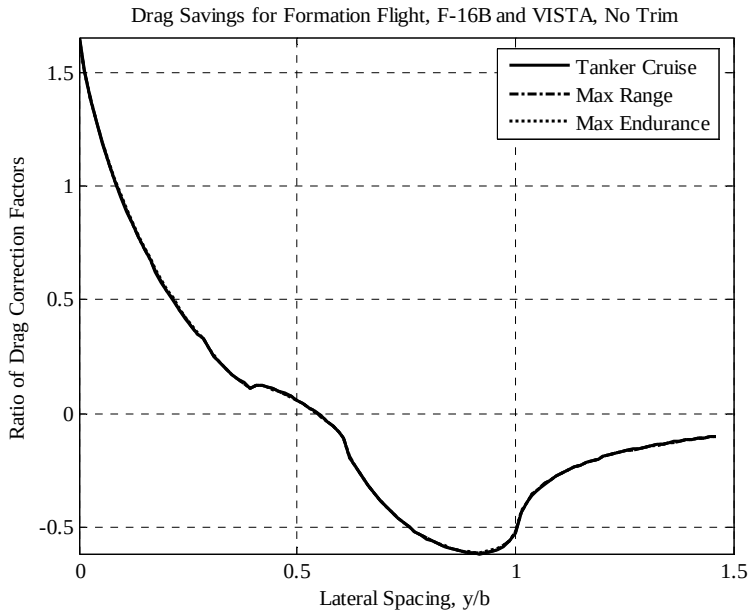

Figure 12. F-16B and NF-16D VISTA in Formation, No Trim, Drag Savings

From Equation 5, a negative value on the graph corresponds to an induced drag savings for the trail aircraft. As shown in Figure 12, the relative induced drag savings for the trail aircraft reached its maximum value at a y/b spacing of 0.925. This position corresponded to previous analyses conducted by both Blake (8:3) and Wagner (35:2-13). Additionally, the zero rolling moment position, from Figure 13, provided a relative induced drag savings of approximately 0.5.

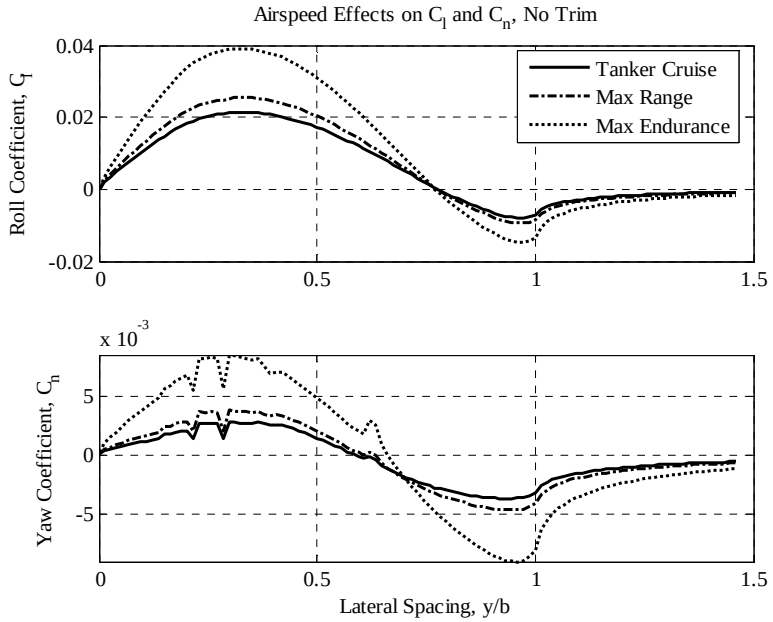

Figure 13. F-16B and NF-16D VISTA in Formation, No Trim, C_l and C_n Values

The trend of the roll coefficients as the aircraft was swept through the span of the lead aircraft remained consistent with those obtained by Wagner (35:2-13). Previous work has not developed the variation of the C_n values. The erratic nature of the C_n values at approximate locations of y/b=0.25 and 0.6, were due to the modified location of the ventral fins in the approximation of the vertical body as a flat plane. The flight control trim analysis was limited in scope to $0.6 < y/b < 1.15$. This area was seen to have the largest magnitude in reduction of the induced drag, as shown in Figure 12.

The relative benefit for all test airspeeds was nearly identical as seen in Figure 12. However, from Figure 13, it can be seen that the slower airspeeds produced larger values in magnitude of the both the roll and yaw coefficients. To truly compare the expected

drag savings, a detailed analysis was conducted with the inclusion of flight control surface trim actuations.

Trim Analysis, F-16 B and NF-16D VISTA Formation

The trim control laws for the F-16 were incorporated into the analysis. The F-16 has three control surfaces working in concert to trim the aircraft in the roll and yaw axes: the rudder, flaperon, and horizontal stabilator. The rudder deflection, δ_r, was independent of the other two control surfaces. From F-16 control logic (15:9-10), it was determined that the flaperon deflection, δ_f, and the horizontal stabilator deflection, δ_s, movements are coupled. The ratio of movement was defined as:

$$\frac{\delta_s}{\delta_f} = 0.294 \tag{19}$$

To determine the magnitudes of trim positions to be introduced into the simulation, a linear approximation was initially assumed with respect to the trim affects:

$$C_l = C_{l_{\delta_a}}\delta_a + C_{l_{\delta_r}}\delta_r \tag{20}$$

$$C_n = C_{n\delta a}\delta_a + C_{n\delta r}\delta_r \tag{21}$$

In this approximation, δ_a was the combined effect of the flaperon and horizontal stabilator deflections. Incremental changes were made to the trail aircraft trim positions and the average change in the C_l and C_n values, for each control input, were approximated to determine the stability derivatives of $C_{l_{\delta_a}}$, $C_{l_{\delta_r}}$, $C_{n\delta a}$, and $C_{n\delta r}$. Subsequently, the magnitude of trim position actuation was determined for each control

surface to effectively trim the aircraft in the roll and yaw axes at each incremental position of the y/b sweep. This linear approximation was accomplished for each discretized point in the lateral spacing.

As expected, from the untrimmed reference case depicted in Figure 13, the slowest airspeed, maximum endurance, required the largest magnitude of trim deflections. As a result, the linear approximation technique used to determine the expected trim positions was inaccurate. Logical manual modifications in the trim positions were induced to effectively negate the larger coefficients present at this airspeed.

For analyzing the trim cases, all three airspeeds provided similar results. Therefore, the following three graphs are representative for all cases. The case described in detail is test case 1, Generalized Tanker Cruise Airspeed. Further graphs of cases 2 and 3 can be seen in Appendix C.

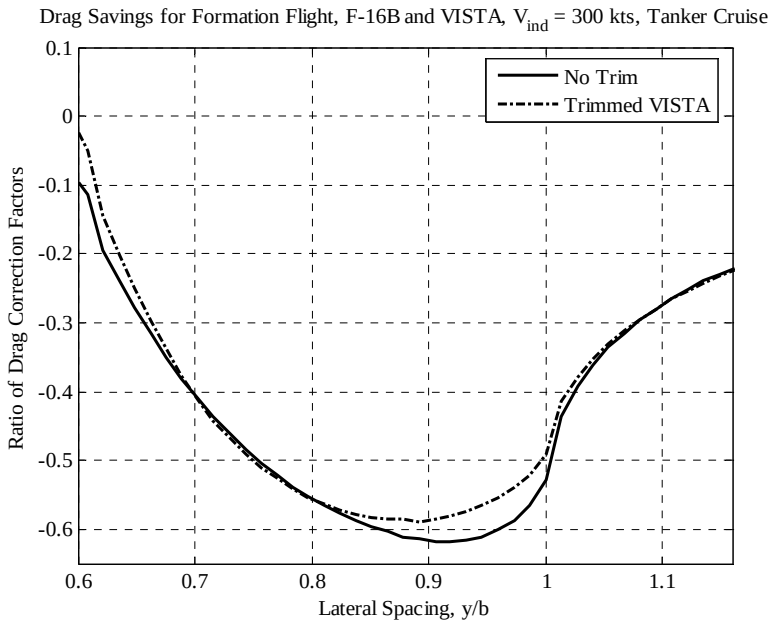

Figure 14. Trimmed Drag Reduction, Tanker Cruise

In the determination of a trimmed aircraft, the magnitude of both C_l and C_n were less than 0.0001, the computational accuracy of the HASC95 output, shown in Figure 15. The flight control surface deflections into the freestream airflow increased the drag of the trail aircraft and decreased the relative drag savings. From Figure 14, the magnitude of R was seen to decrease by approximately 10% with the introduction of trim deflections. This increase was representative of a decrease in the relative savings of formation flight, as compared to the untrimmed case. At the untrimmed maximum savings benefit at 7.5% overlap, the flight control surface deflections required to trim the aircraft were at a maximum, from Figure 16. With the increase in drag associated with the flight controls, the minimum induced drag lateral position changed from approximately 0.925 to 0.865, or from 7.5% to 13.5% wingtip overlap.

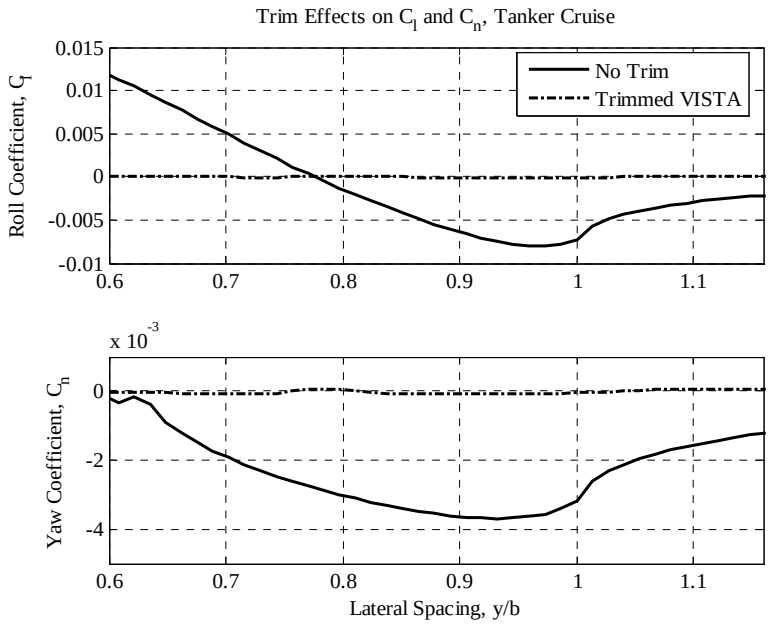

Figure 15. Trimmed C_l and C_n, Tanker Cruise

An additional consideration in the application of flight control trim positions was to ensure that the magnitudes of flight control deflection did not violate the range of motion of the control surfaces. From Figure 16, the flaperon position was seen to have the highest magnitude of –3.5° for this airspeed. Additional investigation of the maximum endurance airspeed, Figure 35, Appendix C, revealed that the maximum trim deflection angle was approximately –6.75° for the flaperon. All control deflections for the area examined were within the limits of the flight controls of the F-16 (30:4).

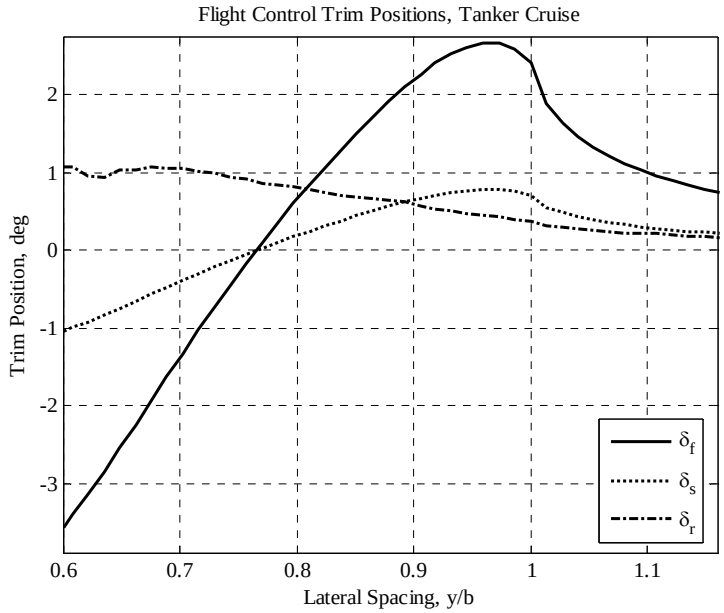

Figure 16. Flight Control Trim Positions, Tanker Cruise

Figure 17 is a combination of all three airspeeds used in the similar formation analysis. The data revealed that the induced drag ratio for the formation decreased as the airspeed decreases. The induced drag was only a portion of the total drag used to determine the power savings benefits, and the power savings was seen to increase as the airspeed decreased. However, to achieve maximum induced drag savings, the relative lateral position of the aircraft remained constant.

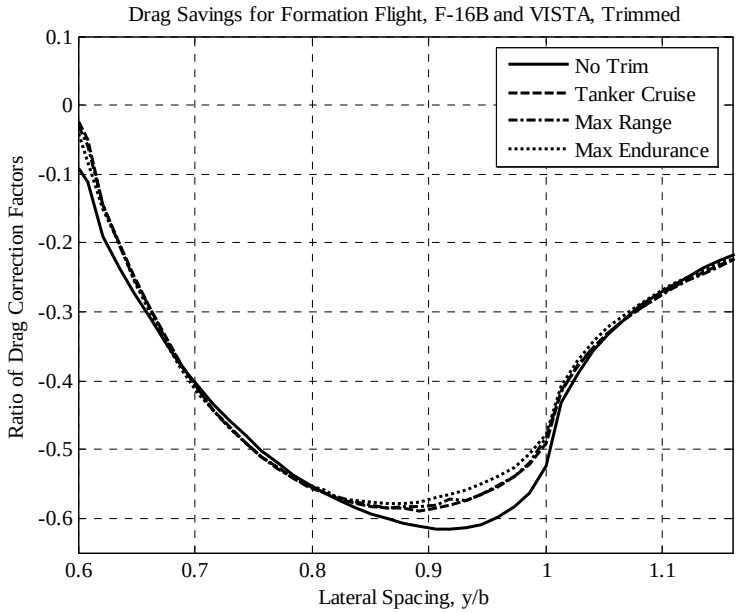

Figure 17. Trimmed Drag Reduction Comparison, All Airspeeds

From Figure 17, the values of R were taken and applied to Equation 9. The following results were produced:

Table 5. Similar Formation Drag Savings

Test Case	y/b	K_{12}/K_0	$C_{D,f}$	$C_{D,f}/C_D$	Percent Savings
1	0.865	-0.5852	0.0232	0.8358	16.419
2	0.865	-0.5846	0.0247	0.7890	21.104
3	0.865	-0.5795	0.0321	0.6585	34.149

Each of the three test airspeeds yielded a 13.5% overlap of the wings for the minimum drag position. This coincides with the determinations of Wagner (35) and Vachon (33), who predicted a 14% and 13% overlap respectively. The percent power

savings was of the same order as their findings for the 300 KIAS examination. Although the induced drag ratio for all airspeeds was approximately equal from Figure 17, the power savings increased considerably as the airspeed decreased: approximately two times greater for a reduction of 90 KIAS. As the lead aircraft decelerated, the coefficient of lift required to maintain level flight and the strength of the trailing vortex increased, resulting in an increased benefit for the trail aircraft. With this analysis of a trimmed two-ship similar formation, it can be seen that considerable gains can be exploited through the trail aircraft flying in proper alignment. As well, this profile was determined to be fully trimmable, allowing for the successful integration of a station-keeping autopilot scheme to truly reap the rewards. As NASA has shown a descent of the trailing vortex, the subsequent flight test of this profile was designed to capture a planer area perpendicular to the direction of flight.

KC-135R and NF-16D VISTA Dissimilar Formation, Untrimmed Solution

The second profile analyzed was a dissimilar formation. The formation consisted of a lead KC-135R and a trail VISTA. This formation was indicative of a tanker ferrying profile of a formation of UAVs. As stated previously, the trailing aircraft flying in a drag reducing position will be able to fly the same profile and require fewer aerial refuelings, or increase the overall range of the formation. With the increased range, the UAVs would be afforded a higher on-station time following this profile.

The simulation was run at 20,000 ft and 300 KIAS for both aircraft using standard-day atmospheric conditions. This airspeed was the only one examined in this analysis. The longitudinal nose-tail separation was set at 6 feet nose-tail separation for the aircraft. This position will provide the capability for the lead aircraft to visually monitor the trail during actual flight. To achieve a valid solution, the step size was chosen to be 15 inches in the lateral dimension. This allowed for a computationally stable result in the lateral analysis. Additionally, as the KC-135R wing has a 7° anhedral angle, the analysis will include variation in the elevation of the trail aircraft to determine the maximum benefit. To effectively capture the elevation of the wing, five discrete vertical positions were selected; vertically aligned with the wing root (173 inches), c.g. (202 inches), 3/4-wing height (225 inches), wing tip (245 inches), and 25 inches above the wing height (270 inches) (24). A depiction of the computational profile is shown in Figure 18.

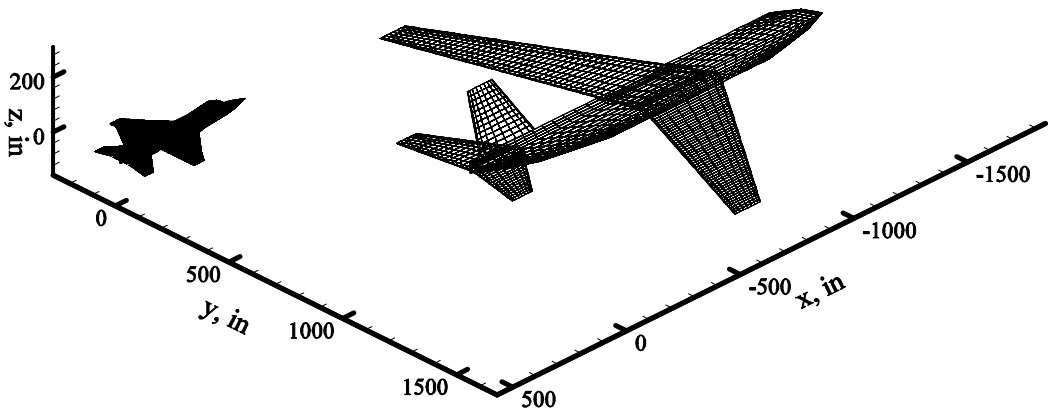

Figure 18. KC-135R and F-16 VISTA Formation

From Figure 19, the computationally best profile for further investigation was seen to be the tip-aligned vertical position. This alignment was assumed to be a result of the linear nature of the HASC95 predictive code. This position achieved a 25% greater benefit than the next best profile. Also shown in Figure 19 was that the assumed lateral position outboard of the #1 or #4 engines, wing stations 545, captured the area representing the greatest benefit. At the minimum spacing of y/b=0.5, the nose of the trail aircraft was aligned with the wingtip of the KC-135. The inboard wingtip of the VISTA was aligned with station 554 of the tanker. At this location, there was a 20 inch overlap of the wingtip into the outboard engine, which extended to approximately wingstation 575. At the maximum benefit position for an untrimmed VISTA, y/b=0.6, there was a 2.5 feet wingtip overlap of the trail plane.

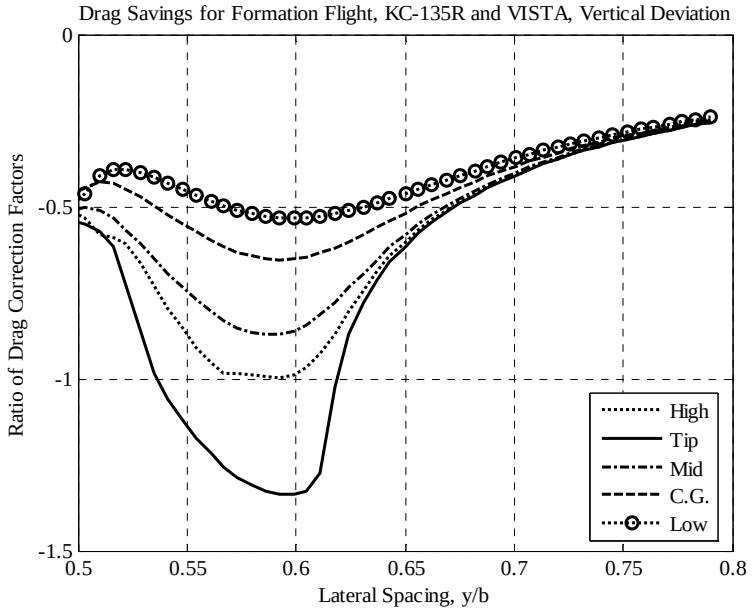

Figure 19. Drag Reduction, KC-135 Vertical Deviation

For the trail aircraft to be in a trimmed flight state, the determination of an optimal position required the negation of the C_l and C_n values shown in Figure 20. The examination into the flight control trim applications will be further discussed in the next section.

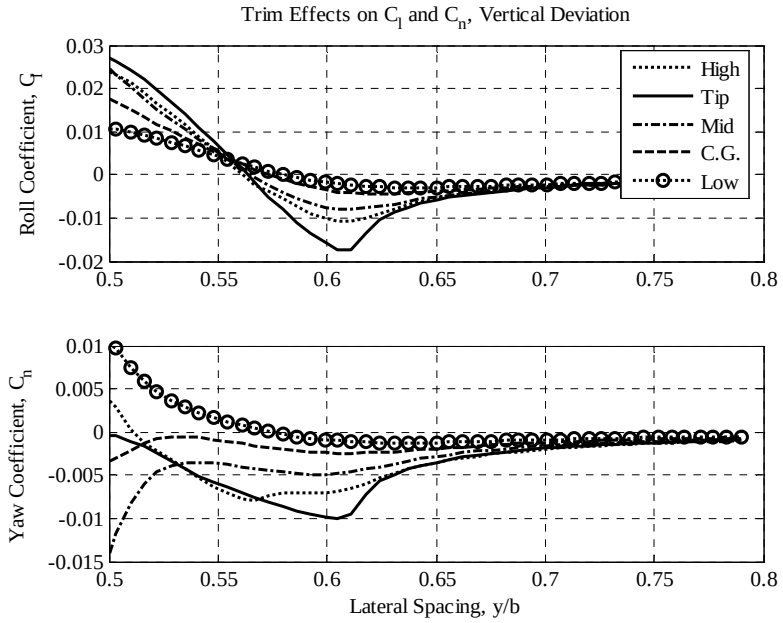

Figure 20. C_l and C_n, KC-135 Vertical Deviation

KC-135R and NF-16D VISTA Dissimilar Formation, Trimmed Solution

The introduction of a trim analysis of the dissimilar VISTA and KC-135 scenario incorporated the same assumptions as the similar formation. The linear approximation of the trim inputs, Equations 20 and 21, was used to approximate the application of control surface deflections. The same limitations were placed on the magnitude of C_l and C_n in

determination of a trimmed state; being less than 0.0001. Given this limit, the trimmed aircraft was analyzed at each incremental step. Figures 21 to 23 represent the data for the trail aircraft.

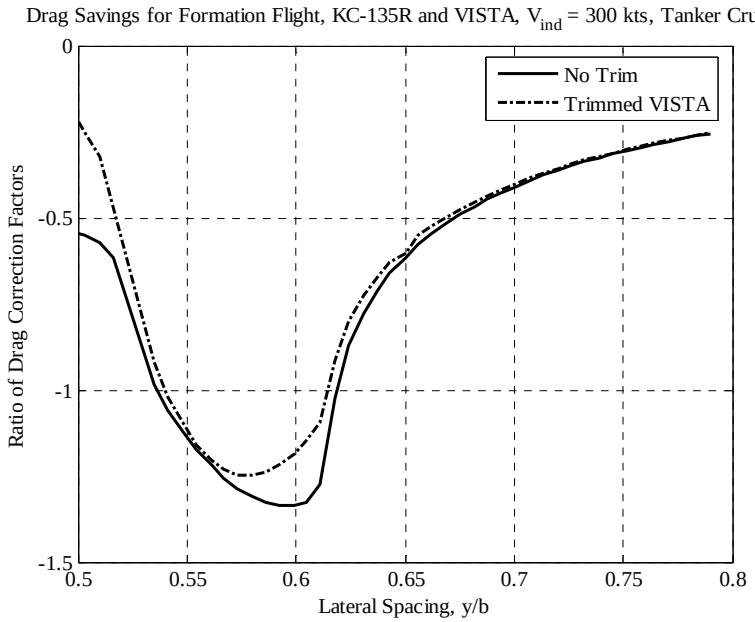

Figure 21. Drag Reduction, Trimmed KC-135, Tip Alignment

From Figure 21, the effects of the trim applications yielded approximately a 5% reduction in the induced drag benefit, as with the similar formation analysis. Also, the lateral spacing shifted inwards, resulting in increased wingtip overlap, from the untrimmed case. This follows the similar aircraft formation analysis. Table 6 summarizes the total drag savings results from Figure 21.

Table 6. Dissimilar Formation Drag Savings

y/b	K_{12}/K_0	$C_{D,f}$	$C_{D,f}/C_D$	Percent Savings
0.580	-1.2479	0.0187	0.7386	26.142

The magnitudes of the roll and yaw coefficients as well as the required flight control surface deflections are shown in Figures 22 and 23.

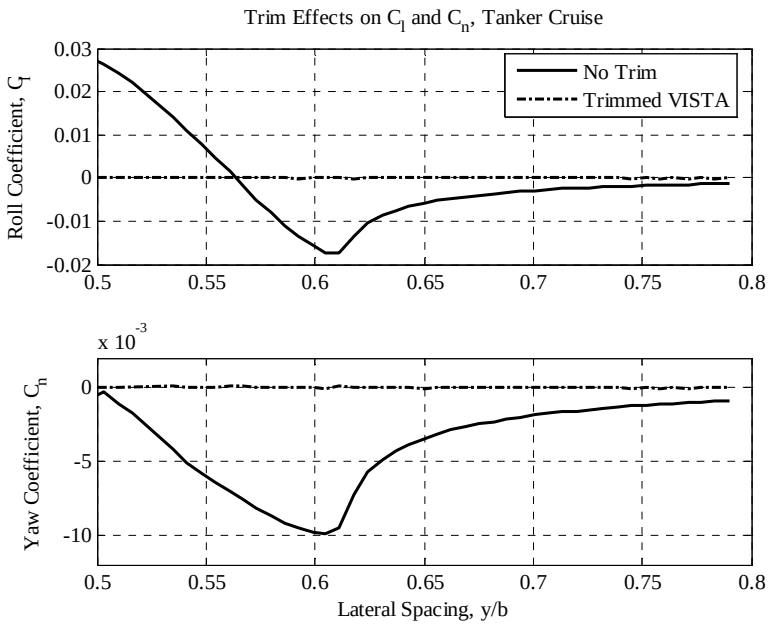

Figure 22. C_l and C_n, Trimmed KC-135, Tip Alignment

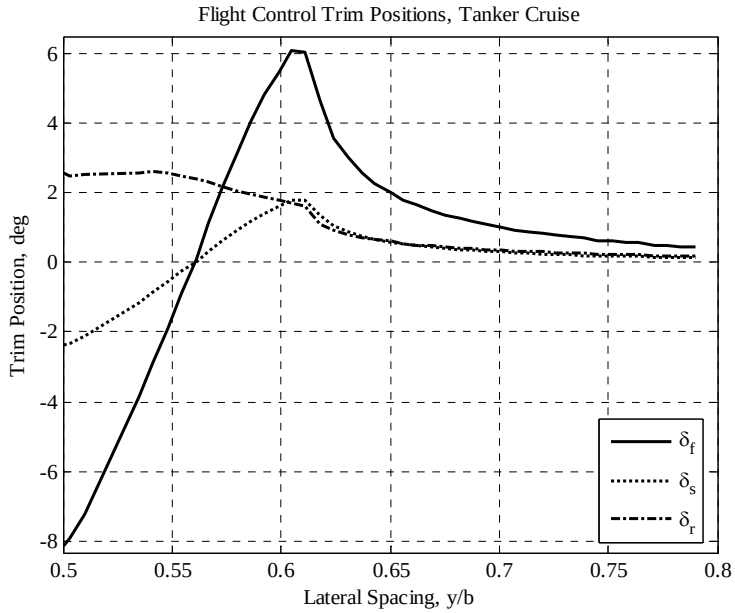

Figure 23. Flight Control Trim Positions, KC-135, Tip Alignment

At the lateral spacing from Table 6, there was an overlap of 62 inches, or approximately 16.67% of the F-16 wingspan. This position resulted in a power savings of 26% for the trail aircraft. As before, the trim positions were within the tolerances of the F-16 control logic. This implies that a station-keeping autopilot is within the capability of the aircraft.

Summary

The two formation profiles, similar and dissimilar, have been analytically examined in this chapter. From the examination, aircraft speed was seen to have no effect on the ideal lateral spacing for an aircraft to fly in order to gain the highest benefit. As the airspeed was decelerated, higher magnitudes of trim control surface deflection

were necessary as a result of the increased vortex intensity of the lead aircraft at a slower airspeed. However, for the similar formation, the power savings for the trail aircraft were determined to range from 16% to 34% as the airspeed reduced by 90 KIAS. For a dissimilar formation, of an aircraft roughly one fourth the size of the lead aircraft, the benefits were increased to 26% for a velocity of 300 KIAS. Neither case impeded upon the flight controller actuator limits of the aircraft with the introduction of trim. The remainder of the paper will focus on the flight test, a similar formation scenario. However, there is shown to be a greater benefit in net power savings with a smaller trailing aircraft flying in formation with a larger mothership having an increased strength of the trailing vortex. The results of this dissimilar analysis have the potential to be further explored in a flight test scenario.

IV. Flight Test

Chapter Overview

The computational analysis determined the induced drag and subsequent power benefit for the trail aircraft flying in a close formation profile. During the flight test, the fuel flow measurement was the primary information used for data correlation. The fuel flow measurements could be calculated as a fuel savings for the system of aircraft. With a suitable engine model, this fuel flow measurement technique was assumed to provide a direct correlation to the predicted drag savings.

The flight test was conducted at Edwards AFB, CA during October and November of 2004. The test team was comprised of three pilots and two flight test engineers from the USAF Test Pilot School (TPS), Class 04A, and one project engineer from the USAF TPS. The author of this thesis served as the project manager for the flight test. The information presented in this thesis can also be found in the test team's final report (25).

The overall objective of the flight test was to determine, from a limited set of positions, the formation position for maximum fuel savings and evaluate how this position changed over three discrete airspeeds. The generalized cruise, maximum range, and maximum endurance airspeeds corresponded to 300, 270, and 210 Knots Calibrated Airspeed (KCAS). Additionally, information was gathered to determine flight control

surface deflections and the pilot workload associated with maintaining spacing while flying in the vortex of another aircraft.

During the planning for the data collection missions, it was determined that the NF-16D VISTA was unable to collect fuel flow data. The formation positions of the analytic solution were modified, and the VISTA was used in the lead, or number one, position. The trail aircraft, an F-16B, was equipped with a Data Acquisition System (DAS) to collect the air data. This formation composition was considered to be similar for the analysis.

Prior to analyzing the flight test, the procedures to fly and reduce the data will be outlined. This chapter starts by detailing the maneuver and positions flown for the data collection. From this, the algorithm used to determine an accurate relative displacement between the aircraft will be summarized. With the resources used during the flight test, the data reduction scheme to resolve a benefit for the trail aircraft will be discussed. Finally, the method to determine the trimmed flight control surface deflections will be described.

Flight Test Procedures

For determining the relative fuel savings for a formation of two aircraft, a flight test technique similar to Wagner's was used (35:3-5). This method was repeated for each point in the positional test matrix, described in the next section. Maintaining a set vertical separation and increasing relative wingtip overlap, then lowering the vertical

spacing and progressing from lesser to higher amounts of wingtip overlap, varied the spacing. During the test, the acceptable bounds for data collection were between 10,000 and 30,000 feet in altitude and established within 10 knots of the test airspeed. Once established, the tolerances for the parameters were ±50 feet and ±2 knots.

With the formation established on test conditions, altitude and airspeed, the test aircraft was flown at a set longitudinal spacing of 200% wingspan, outside of any wingtip overlap. The trail aircraft maintained a constant vertical position and increased wingtip overlap to the desired position. Once stabilized, a minimum of 30 seconds of consecutive DAS data was collected in the vortex position. Figure 3 represents the formation geometry used during the flight test, but does not depict the specific positions flown.

Following flight in the vortex, the trail aircraft cleared the lead aircraft to a lateral spacing of greater than five wingspans line abreast; effectively clear of any vortex interactions. The test aircraft maintained the reduced power setting and test altitude and allowed the airspeed to decelerate until a stabilized condition was achieved. This was defined as being less than 1 KCAS per 10 seconds decrease in airspeed. Maintaining constant altitude, the test aircraft increased the throttle setting and re-established the test airspeed observed while flying in the vortex position. Data at these stabilized conditions were collected for a minimum of 30 seconds.

Positional information was collected on board each aircraft through the use of production GPS receivers and antennas that were installed in the aircraft, further discussed in the next section. The GPS receivers were not accessible during flight. As such, the receivers were initialized on the ground prior to engine start, and positional data

were collected throughout the entire mission. No real time display of relative displacement was available to the pilots.

The goal of the flight test was to capture a planar cross-section of fuel savings, perpendicular to the direction of flight at a constant longitudinal spacing of two wingspans. At a constant longitudinal spacing of 200% wingspan, the planned lateral and vertical separations are shown in Table 7. The test matrix was centered about the assumed point of greatest benefit; a lateral overlap of 13.5%, from the analytic solution in Chapter 3, and a -6% vertical separation, from NASA flight test results. All spacing was determined from a body axis reference frame with the origin on the nose of the trail aircraft. A negative vertical separation implies that the trail aircraft is flying in a position lower than the lead aircraft.

Table 7. Planned Formation Positions

Position Number	Wingspan Overlap, y/b (percent)	Wingspan Overlap (in)	Vertical Separation, z/b (percent)	Vertical Separation (in)
1	7.5	28	0	0
2	13.5	50	0	0
3	18.3	68	0	0
4	7.5	28	-6	- 22
5	13.5	50	-6	- 22
6	18.3	68	-6	- 22
7	7.5	28	-12	- 44
8	13.5	50	-12	- 44
9	18.3	68	-12	- 44
10	0	0	0	0
11	0	0	-6	-22
12	0	0	-12	-44
Note: 100 percent indicates 372 inches or 31 feet				

With no real-time positional information displayed to the pilots, an estimation of the planned positions was accomplished prior to the test missions. Photographs were taken from the pilot's eye position at each location. These provided the capability to assess the visual references available to the pilots for maintaining a stable formation position. Figure 24 is a photograph of the NF-16D VISTA taken for formation position number 2, from Table 7.

Figure 24. Trail Aircraft Visual References

For the forward references, the relative position of the noseboom with respect to the three static discharge wicks on the aft section of the wing was used. For the aft references, the relative position of the horizontal stabilizer with respect to the doors on the underside of the aircraft assisted in the pilot's positional assessment. By using these visual references,

the pilot's were able to maintain a constant relative displacement to the lead aircraft. The data collected at these positions were used to determine the true displacement between the aircraft.

Positional Determination

To determine the relative displacement, a GPS receiver and antenna were installed in each aircraft. The receiver chosen for the flight test was the Ashtech Z-Extreme™. This is a dual-frequency, carrier-phase capable receiver. Using data collected during the mission, the spacing between the aircraft was determined from a production differential GPS algorithm: Waypoint Consulting's GrafMov™ program. Using the post-processed data, the receiver attained a position with centimeter-level accuracy (5:5).

The positional information was determined in an inertial Earth-Centered, Earth-Fixed (ECEF) reference frame. A relative ECEF displacement vector between the two antennas was attained from the production software. A kinematic GPS solution was used in the processing of the positional data. Further information regarding the operation of the computer code can be found in the user's manual (36). Using aircraft parameters of heading, pitch, and roll angles, the ECEF coordinates were transformed into a body axis reference frame by Equation 22. The body axis reference frame was a conventional orthogonal system with the x-axis positive out the nose of the aircraft, the y-axis positive out the right wing, and the z-axis positive out the bottom of the aircraft.

$$\Delta\vec{X}_b = T_{NED\rightarrow Body} T_{ENU\rightarrow NED} T_{ECEF\rightarrow ENU} \Delta\vec{X}_{ECEF} \qquad (22)$$

The first transformation matrix changed the displacements from an inertial ECEF reference frame to a local-level, East-North-Up (ENU), reference frame (23:119). The latitude, ϕ, and longitude, λ, were attained from the trail aircraft's GPS receiver positions.

$$T_{ECEF \to ENU} = \begin{bmatrix} -\sin\lambda & \cos\lambda & 0 \\ -\sin\phi\cos\lambda & -\sin\phi\sin\lambda & \cos\phi \\ \cos\phi\cos\lambda & \cos\phi\sin\lambda & \sin\phi \end{bmatrix} \tag{23}$$

The second transformation matrix was to convert the position from the ENU to an intermediate North-East-Down (NED) reference frame.

$$T_{ENU \to NED} = \begin{bmatrix} 0 & 1 & 0 \\ 1 & 0 & 0 \\ 0 & 0 & -1 \end{bmatrix} \tag{24}$$

The final transformation matrix was to obtain positional information in the conventional body axis reference frame (27:105). The yaw angle, Ψ, pitch angle, Θ, and roll angle, Φ, were determined from the recorded DAS information. The data parameters of interest to the analysis are summarized in Table 9, Appendix E. The measured heading angle was corrected for a magnetic deviation of 14° east variation to obtain true heading, or the yaw angle.

$$T_{NED \to Body} = \begin{bmatrix} \cos\Psi\cos\Theta & \sin\Psi\cos\Theta & -\sin\Theta \\ \cos\Psi\sin\Theta\sin\Phi - \sin\Psi\cos\Phi & \sin\Psi\sin\Theta\sin\Phi + \cos\Psi\cos\Phi & \cos\Theta\sin\Phi \\ \cos\Psi\sin\Theta\cos\Phi + \sin\Psi\sin\Phi & \sin\Psi\sin\Theta\cos\Phi - \cos\Psi\sin\Phi & \cos\Theta\cos\Phi \end{bmatrix} \tag{25}$$

The result of Equation 22 was a body axis displacement vector between the two GPS antennas. However, the antennas were located at different positions for each of the aircraft. This discrepancy was accounted for in Equation 26, which was used to

determine a body axis displacement from the nose of the trail aircraft to the nose of the lead aircraft.

$$\Delta\vec{X} = \Delta\vec{X}_b + \vec{X}_{\text{antenna}048} - \vec{X}_{\text{antenna}635} \tag{26}$$

In relation to the nose of the aircraft, the position of each antenna was determined to be the following body-axis vectors (in meters):

$$\vec{X}_{\text{antenna}635} = \begin{bmatrix} -4.5323 \\ 0.0000 \\ -0.8446 \end{bmatrix} \quad \vec{X}_{\text{antenna}048} = \begin{bmatrix} -10.0690 \\ 0.0000 \\ -1.1433 \end{bmatrix}$$

Equation 26 provided a displacement vector in the body axis reference frame. This position was used to subsequently correlate fuel savings, flight control surface deflections, and pilot workload to a point in space while maintaining a stable platform in a vortex position.

Fuel Savings Analysis

For the flight test, the fuel savings was correlated to a relative displacement of the aircraft by three techniques. A fuel flow method analyzed the difference in fuel flow between positions where the test aircraft was stabilized in the vortex and where it was clear of the vortex at the test airspeed. A core engine speed method analyzed differences in engine speed for the same conditions. Lastly, an airspeed method used the difference between the calibrated airspeed of flight clear of the vortex at a reduced power setting and the calibrated airspeed of the trail aircraft while in the vortex position. During the

stabilized portion of the flight test technique, flight test data, shown in Table 9, Appendix E, were collected by the trail aircraft's DAS.

The fuel flow method provided a direct correlation to the fuel savings predicted from the analytic power saving's results. The fuel flow method compared a change in the fuel flow reading of flight in the vortex with respect to flight in the freestream conditions to arrive at fuel savings estimations. For this technique, variations in the energy height of the trail aircraft were incorporated in the calculations (9). The energy height was used to determine specific excess power and subsequently to correct the measured fuel flow for minor variations in altitude and airspeed during the data collection periods. Equation 27 determined the energy height, E_s, of the aircraft (4:335):

$$E_s = h_p + \frac{1}{2g} V_t^2 \tag{27}$$

where h_p is *altitude*, V_t is *true airspeed* and g is the *gravitational constant*.

The DAS parameters were used to determine the energy height approximation, and a second order approximation was applied to the energy height as a function of time. Specific excess power, P_s, was then evaluated as the first derivative of the energy height approximation with respect to time, Equation 28, at each discrete point (4:337).

$$P_s = \frac{d}{dt}(E_s) \tag{28}$$

Having determined the P_s of the aircraft, a fuel flow correction, $\Delta \dot{w}_f$, was determined by Equations 29 to 31 (9):

$$n_{FPA} = \frac{P_s}{V_t} \tag{29}$$

$$F_{ex} = n_{FPA} \cdot W \tag{30}$$

$$\Delta \dot{w}_f = -F_{ex} \cdot TSFC \tag{31}$$

where n_{FPA} is *flight path acceleration*, W is *weight*, F_{ex} is *excess thrust*, and $TSFC$ is *Thrust Specific Fuel Consumption*, assumed to equal one for this evaluation.

The fuel flow correction was applied to each fuel flow measurement as shown in Equation 32. This resulted in fuel flow measurements corrected for energy height.

$$FF_{E_{S_{corr}}} = FF_{measured} + \Delta \dot{w}_f \tag{32}$$

Having corrected the measured fuel flow reading for variation in the specific energy, the relative fuel savings, FS, for each position flown was determined by Equation 33. In this expression, "m" represents the number of data points collected in the vortex position, "vor," and "n" represents the number of data points collected while operating as a single ship, "ss," clear of the vortex. The fuel flow data used in this calculation was determined from the pilot's stabilized estimation during the flight in the vortex position.

$$FS = \frac{\frac{\sum_{i=1}^{n} FF_{E_{S_{corr\ ss}}}{}_i}{n} - \frac{\sum_{i=1}^{m} FF_{E_{S_{corr\ vor}}}{}_i}{m}}{\frac{\sum_{i=1}^{n} FF_{E_{S_{corr\ ss}}}{}_i}{n}} \text{x}100 \tag{33}$$

The measured fuel flow reading of the DAS used a production fuel flow meter. From Table 9, the resolution of the reading was ±20 pounds per hour with an uncertainty of ±100 pounds per hour. For the generalized tanker cruise condition, the predicted fuel flow for an F-16 was 2,800 pounds per hour (14:C4-33). The inherent uncertainty in the numerator of Equation 33, the difference of the fuel flows, was up to 200 pounds per hour, corresponding to an overall resolution of ±7% for the fuel savings calculations. To minimize the impact of this error source, engine speed and airspeed changes were collected to correlate the relative fuel savings of the formation.

The engine core speed had a resolution of ±0.01% revolutions per minute (rpm) and the calibrated airspeed had a resolution of ±0.07 knots. It was determined that for the test altitude of 20,000 feet, a 2% change in rpm corresponded to a 5% change in fuel flow (24:64). Likewise, for the calibrated airspeed, a 10 knot difference was indicative of a 5% change in fuel flow (14:C4-33). These were expected to provide usable analyses based on the higher resolution of the measurements and to provide a physical correlation to the fuel savings calculations.

Both the engine speed and airspeed techniques were accomplished in a similar manner. No correction was applied to the measured values. The engine speed analysis compared a reduction of the core rpm while flying in the vortex to the core rpm while flying clear of the vortex at the test airspeed. The airspeed analysis was a difference of the airspeed while flying clear of the vortex at the reduced power setting to the test airspeed. These calculations were accomplished as follows:

$$\Delta RPM = \frac{\sum_{i=1}^{n} RPM_{ss_i}}{n} - \frac{\sum_{i=1}^{m} RPM_{vor_i}}{m} \quad (34)$$

$$\Delta AS = \frac{\sum_{i=1}^{m} V_{c_{vor_i}}}{m} - \frac{\sum_{i=1}^{n} V_{c_{ss_i}}}{n} \quad (35)$$

This section discussed the methods used to conduct the fuel savings analysis for the flight in the close formation position. Additionally, the trimmed flight control surface deflections were determined using the DAS data. The method used for this analysis is presented in the next section.

Trimmed Flight Control Surface Deflection Analysis

The HASC95 analysis provided an estimate for the expected flight control surface deflections required to trim the aircraft in the roll and yaw axes. The flight control surface deflections were collected for the test aircraft. The resultant flight control surface deflections were calculated using the DAS data to correlate the surface deflections with the relative position of the aircraft in formation.

The resultant flight control surface deflections were calculated as the difference of the effective flight control while operating in the freestream conditions to the effective flight control deflection while flying in the vortex. The resultant flight control deflection was chosen for a direct comparison with the HASC95 prediction. This method accounted for any asymmetries that existed in the test aircraft leading to residual surface deflections

for a normal trimmed state. The effective flight control deflections for the horizontal stabilizer, δ_s, flaperon, δ_f, and rudder, δ_r, were defined as:

$$\delta_{s\,\text{effective}} = \frac{\delta_{slt} - \delta_{srt}}{2} \tag{36}$$

$$\delta_{f\,\text{effective}} = \frac{\delta_{f\,lt} - \delta_{f\,rt}}{2} \tag{37}$$

$$\delta_{r\,\text{effective}} = \delta_r \tag{38}$$

where "lt" is the left surface and "rt" is the right surface.

Summary

The algorithms used to determine the relative spacing of the formation, the fuel savings, and flight control surface deflections have been described in this chapter. Additionally, a subjective evaluation of the pilot's workload while manually flying the formation position was made. The workload was assessed during flight after flying in the stabilized position using a modified 7-point workload assessment scale (2:3). The workload assessment scale is included in Table 10, Appendix F. Using these techniques, the results of the flight test will be presented in the following chapter.

V. Flight Test Results

Chapter Overview

This chapter will detail the results of the flight test using the methods outlined in the previous chapter. First, the fuel savings analysis and positional determination will be discussed. Following that, the flight test results will be compared to the HASC95 predictions from the analytic analysis of a similar formation. Finally, an assessment of the pilot workload and comments regarding flight in the vortex position will be evaluated. Prior to analyzing the flight test results, a summary of the missions flown will be presented.

Flight Test Mission Summary

The flight test was flown to evaluate the position for greatest fuel savings benefit and determine how this position changed flying three discreet airspeeds; generalized cruise of 300 KCAS, maximum range of 270 KCAS, and maximum endurance of 210 KCAS. Five two-ship missions were flown in October and November of 2004 at the AFFTC, Edwards AFB, CA in support of this test totaling 13.8 hours of flight test. Two missions were flown for the generalized cruise and maximum range airspeeds, and one mission was flown to evaluate the maximum endurance airspeed. However, during the flight test, the only missions that captured DAS flight data for the trail aircraft were for

the two missions flown at the generalized cruise airspeed. The lack of recorded angular parameters for the remaining airspeeds prevented an accurate positional determination. An approximation for the maximum range and maximum endurance airspeeds, based on recorded information from the heads-up display, was accomplished to determine the angular measurements for the coordinate transformation. The fuel flow readings were recorded during flight from the production aircraft gauges. These resulted in estimations of the position and fuel savings for the maximum range and maximum endurance test airspeeds.

The core engine rpm reading, taken from the production cockpit gauges during flight, was unusable due to the resolution. Additionally, the airspeed method for the fuel savings analysis was not suitable for these test conditions, as the aircraft began the maneuver at or near the minimum of the thrust required curve. Following flight in the vortex, and subsequent deceleration at a reduced power setting, the airspeed continued to decay until the aircraft's angle-of-attack limiter was reached, requiring pilot intervention. The reduced throttle setting was below that required to maintain level flight.

The estimations for the 270 and 210 KCAS missions are provided in Tables 16 and 17, Appendix G. Two missions were flown for the generalized cruise airspeed, and the results for these two missions will be presented in this chapter.

Fuel Savings Analysis

The flight test determined the relative displacement of two aircraft and analyzed the fuel savings associated with the formation. The relative displacement was determined through the use of differential GPS solution processed post-flight to provide an accurate position of the aircraft. The fuel savings solution used three techniques for analysis. The first was based on direct measurement of the fuel flow of the test aircraft stabilized in the vortex of the lead aircraft and stabilized in the freestream conditions, clear of any vortex interactions. The second analyzed changes in core engine speed for the same conditions. The third examined the difference between the calibrated airspeed of flight clear of vortex interactions at a reduced power setting and the calibrated airspeed while stable in the vortex position.

The combined results for the fuel flow and engine speed techniques are shown in Figure 25. All test points were flown at a longitudinal spacing of 2.2% ±0.2% wingspan of the lead aircraft. For the observed longitudinal positions, fuel savings as a function of longitudinal separation was not considered. Numerical results can be found in Table 13, Appendix G.

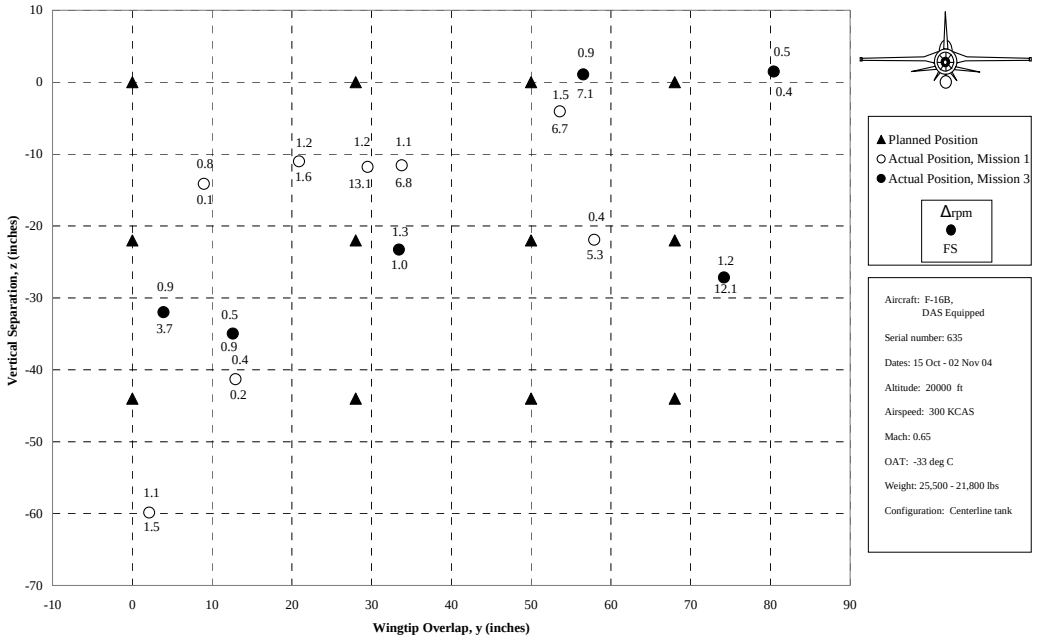

Figure 25. 300 KCAS Flight Test Results

The triangles represent the planned matrix test positions, from Table 7, and the circles correspond to the actual positions flown, as determined by the differential GPS solution. The number above the test point represents the reduction in engine speed, while the number below the point represents the determined fuel savings.

Using the fuel flow technique, the optimal formation position was not precisely determined. From Figure 25, the region of greatest benefit was bounded by 7.9% to 19.9% wingtip overlap and a –3.2% to –7.3% vertical separation to the lead aircraft. 100% corresponds to 372 inches or 31 feet. The observed fuel savings at these bounds were determined to be 13.1% and 12.1% with an uncertainty of ±7%. If these fuel flow measurements were valid, the calculated fuel savings was significant for the trail aircraft of a similar formation. The calculated fuel savings for all positions was determined to be

positive: the trail aircraft was realizing a benefit as a result of flight in the vortex. To correlate these calculations, the engine speed and airspeed methods were also completed.

Despite the increased resolution of the airspeed and engine rpm, the automatic engine tuning of the Digital Electronic Engine Control (DEEC) impaired these two techniques. The DEEC installed on the F-16B F100-PW-220 engine operated in the engine's primary operating mode (13:1-56). In the primary operating mode, the DEEC scheduled fuel flow and controlled the core engine rpm through inputs to the compressor inlet variable vanes. These changes in operating parameters of the engine were most apparent after a delay of approximately ten seconds following an adjustment to the throttle position. Stable engine parameters were difficult to achieve, and power corrections were required as a result of the self-tuning properties of the DEEC. The secondary operating mode of the engine does not trim the engine for optimal performance and engine speed is solely a function of throttle position. For future evaluations in aircraft with this type of engine, the use of the secondary operating mode should be considered. The DEEC-induced corrections adversely affected the results of the engine speed and airspeed evaluations.

The engine speed analysis provided no definable region of greatest benefit, from Figure 25. The two points of greatest benefit for the fuel flow technique resulted in a reduction of 1.2% ± 0.1% using the engine speed technique. A correlation between these two techniques was expected to exist. Figure 26 illustrates that there was no significant correlation between the two methods. The DEEC added ambiguity to the engine speed method by inducing constant, uncommanded changes to the engine rpm. Although the

uncertainty in the fuel flow technique was an order of magnitude greater than the engine speed technique, the fuel flow method provided the most valid trend information.

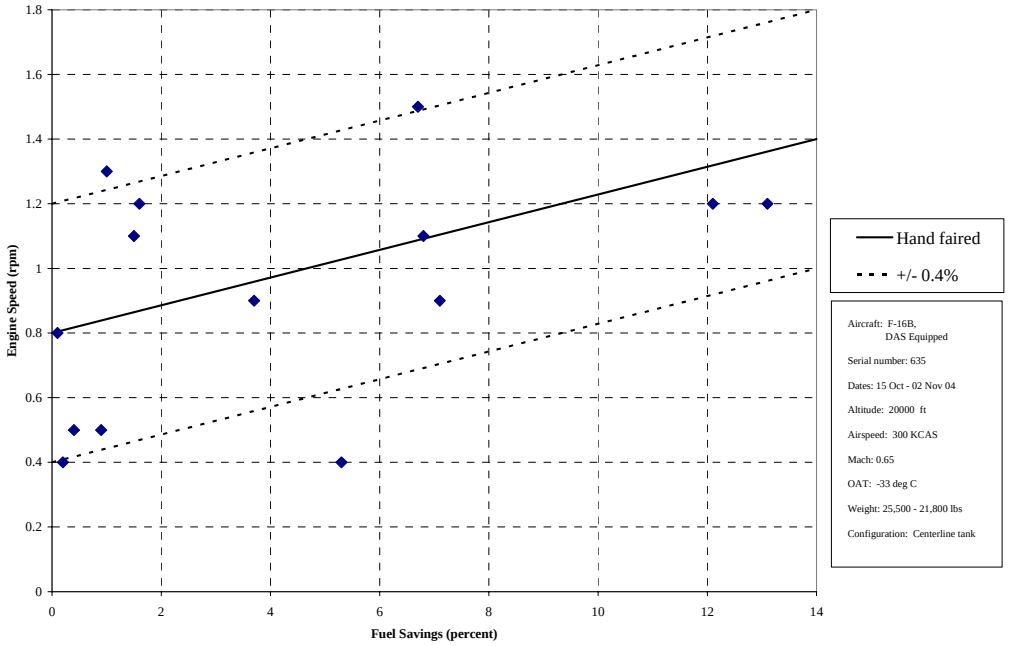

Figure 26. Fuel Savings and Engine Speed Correlation

The airspeed method was found to be more sensitive to the DEEC effects. To maintain proper spacing, the pilots were required to make small, constant throttle corrections. If the last throttle input resulted in a reduction in power, the airspeed deceleration was excessive. The resulting airspeed deviations were not indicative of the reduced power required in the vortex position and the DEEC corrupted the measurements. The airspeed method results can be found in Table 13, Appendix G. As a result, the airspeed method was assessed to be inconclusive and incompatible with the primary operating mode of the F100-PW-200 engine.

The test results were inconsistent between the fuel flow, engine speed, and airspeed methods. The DEEC rendered the engine speed and airspeed methods ineffective. The fuel savings method, although having the greatest uncertainty, provided useable trend information for the position of greatest benefit. However, a precise determination of the position of optimal fuel savings could not be made, except by defining a region of apparent benefit. A more accurate fuel flow reading would be required to obtain greater confidence in the test results. An improved instrumentation system, providing a fuel flow measurement with higher resolution, would be required prior to attempting a similar test. The next section will compare the results of the flight test to the HASC95 predictions.

HASC95 Prediction Assessment

The HASC95 provided predictions of the power savings by computing the change in induced drag for the formation while the flight test computed a fuel savings based on the change in fuel flow from flight in the vortex to flight in the freestream. The power savings was considered to be a direct comparison to the fuel savings. The variations in vertical positioning were not predicted by HASC95 due to the linear VLM used in the approximation. This section will compare the predictions of the optimal formation position, its associated fuel savings, and control surface deflections from the HASC95 analysis to the results of the flight test.

Flight test determined that optimal lateral wingtip overlap was bounded between 7.9% to 19.9% overlap. The HASC95 analysis in Chapter 3 predicted an optimal lateral position of 13.5% wingspan overlap for the similar formation. Though the predicted optimal lateral position was near the median value of the range determined from flight test, the actual position of greatest fuel savings could not be precisely determined from test results.

As no solution was found for the position of greatest fuel savings from flight test, the HASC95 predicted maximum 16.4% fuel savings was not evaluated. For the flight test's two points of maximum benefit, at 7.9% and 19.9% wingtip overlap, the realized fuel savings were 13.1% and 12.1%, respectively, with a resolution of ±7%. Predictions for the similar formation's power savings were made using the results presented in Figure 13. The predictions were 14.3% and 15.6%, respectively with a difference between observed and predicted values of less than 4.0% fuel savings. With the limitations on the resolution of the fuel flow measurement, the HASC95 solution compared favorably with the flight test results for calculating the benefit for the trailing aircraft of the similar formation.

As previously discussed, the computational model was trimmed for zero roll and yaw coefficients to improve the accuracy of its fuel savings assessments. Flight control deflections resultant from flying in the lead aircraft's vortex increased the drag experienced by the trail aircraft which, in turn, decreased the fuel savings benefit. During testing, flight control inputs were minimized while flying in the vortex and resultant surface deflections were determined. Predicted and flight test results for the two points

of maximum benefit from the fuel savings analysis are presented in Table 1. The software predictions had a 1.1° maximum magnitude in deviation from observed flight control surface deflections. The HASC95 solution was satisfactory in predicting the flight control surface deflections for trimmed flight in the vortex position.

Table 8. Resultant Flight Control Surface Deflections, 300 KCAS

Position	$\delta_{r_{\text{resultant}}}$ (deg)	$\delta_{s_{\text{resultant}}}$ (deg)	$\delta_{f_{\text{resultant}}}$ (deg)
Mission 1 Run 3	0.4	0.5	1.7
HASC95 Prediction	0.4	0.7	2.5
Deflection Difference	0.0	-0.2	-0.8
Mission 3 Run 3	0.3	0.5	1.8
HASC95 Prediction	0.8	0.2	0.7
Deflection Difference	-0.5	0.3	1.1
Uncertainty	0.3	0.6	0.4

The predictions of the optimal formation position, associated fuel savings, and control surface deflections were compared between the HASC95 analysis and the flight test results. The flight test results were limited as a result of the resolution of the fuel flow measurement and an evaluation of the analytical analysis technique was not accomplished. From the results of the flight test, the HASC95 predictions compared favorably to the fuel savings benefit and the flight control deflections required to trim the aircraft. Although providing favorable results, further flight test would be required to validate the analytic technique in the prediction of the fuel savings benefits for an aircraft formation. An additional evaluation of the workload assessment and pilot comments to manually fly in the vortex position will be discussed in the next section.

Pilot Comments and Ratings

The test team was comprised of three experienced pilots familiar with flying close formation, but not specifically in the vortex position. The pilots' operational experience was in F-15, F-16, and F/A-18 aircraft, and all were familiar with flying the F-16. The relative displacement between the aircraft was maintained using the visual references described in the previous chapter and a workload assessment was made at each position during flight. The determination of the required workload to fly in this position was made using the 7-point rating scale shown in Table 10, Appendix F.

In general, pilot comments and ratings indicated the workload to maintain a stable position in the vortex was high. From Tables 15 through 17, the pilot assigned workload varied between a 3 and 6 depending on the pilot and position flown. The same pilot assessed Missions 1 and 4. The remaining two pilots evaluated Missions 3 and 5. Pilots could communicate using the radio and cockpit intercom, and were able to scan cockpit instruments, but were otherwise focused on flying the vortex formation positions. These results did not vary with airspeed when compared to the same pilot at different speeds, and no learning curve was noted between the first and second flight for the same pilot. The high workload to maintain position was a result of the effects of the DEEC and the use of visual references to maintain position.

Comments captured following the flight assessed that the lateral and vertical separations were easier to control than the longitudinal separation. These comments were validated in the differential GPS solution, which indicated a lateral and vertical tolerance

of ±7 inches, while the longitudinal performance was ±26 inches. The self-trimming properties of the DEEC required constant throttle corrections to maintain the desired longitudinal position. Once stabilized, the small throttle corrections were generally ±1° variations in the power lever angle, from DAS data. After making a correction, the DEEC trimmed the engine to a different internal engine speed, and the pilot was required to make a subsequent correction to the power lever angle in order to maintain the desired spacing. These constant changes in throttle setting increased pilot workload while decreasing task performance. In addition to the DEEC effects, the workload was impacted by the use of visual references to maintain position.

The photographs of the lead aircraft at each of the planned test positions assisted the pilots in determining the desired longitudinal and lateral spacing. The test matrix photographs were based on a level angle of attack with the lead aircraft on the ground with the landing gear down. As a result, the vertical spacing was difficult to assess during flight due to angle of attack effects. The pilot was required to estimate the desired vertical spacing based on an evaluation of the lead aircraft pilot's helmet position in relation to the horizon. In all three dimensions, pilots were required to react to changes in line-of-sight and closure with the lead aircraft, leading to a high workload to visually maintain the vortex position.

In general, a more accurate means of station keeping would be desired for formation flight in the vortex of a lead aircraft. A display of relative position changes prior to visual perception by the pilot would increase station-keeping accuracy, thus reducing pilot workload. A flight director display, to visually present variations of

positional trend information, would be suited for this application, providing the pilot cues to maintain the optimum formation position in all axes.

In addition to the planned visual formation cues, pilots were able to sense the vortex position by the roll force required while positioning the aircraft in the vortex. The variation in rolling moment was similar to that shown in Figure 12 as the pilot traversed the vortex in the lateral direction. Pilots sensed the region of greatest vortex interaction, independent of the visual cues. This region was qualitatively assessed as a spacing of 1 foot vertical by 3 feet lateral, and appeared to coincide with the observed fuel savings. Despite the ability to sense the region of apparent savings, the high workload of the vortex position for manual flight would be unsuitable for the prolonged periods required to truly realize the benefits of this position.

Summary

The results of a similar formation profile to include the determination of the optimal lateral spacing for greatest fuel savings benefit, a comparison to the analytical HASC95 predictions, and an assessment of the pilot workload have been examined in this chapter. The evaluation of the flight test was adversely affected by only two of the five missions collecting flight test instrumentation data, which allowed for the investigation of the generalized cruise airspeed, 300 KCAS. Additionally, the 7% resolution of the fuel savings calculation was on the same order of magnitude as the determined results and the self-trimming properties of the engines impacted the evaluation.

The flight test was unable to allow a determination of the exact lateral spacing required to attain the greatest fuel savings benefit for flight in the vortex of a lead aircraft. However, fuel savings of 13% and 12% ±7% were observed for a wingtip overlap bounded by 7.9% to 19.9% wingtip overlap. As such the results of the HASC95 analysis were unable to be compared for the lateral spacing. For the 300 KCAS airspeed, there was an apparent downward shift in the vortex. For a longitudinal spacing of two wingspans, this vertical shift was bounded between 3.2% and 7.3% of the wingspan below the lead aircraft. The analytic power savings and flight control surface deflections compared favorably to the flight test results at these locations. Further flight test of the profile would be necessary to validate the HASC95 analysis as a low-cost predictive algorithm.

Additionally, the workload to manually fly in the vortex position was assessed as high as a result of the engine effects and the lack of real-time positional displays to the pilots. The pilot while flying in the vortex sensed the area of apparent greatest benefit. However, high pilot workload would still require significant pilot attention, prevent accomplishment of other cockpit tasks, and increase fatigue during long periods of formation flight. For this reason, the military utility of the vortex formation position would be low for the objective of saving fuel during routine operations. Alternatively, a UAV with a suitable flight control system could be programmed to maintain the optimum position without regard to workload and routinely realize significant fuel savings.

VI. Conclusions and Recommendations

The purpose of this thesis was to further define the position of greatest fuel savings benefit for the trail aircraft of a two-ship formation. The analytical analysis included the capability to trim the aircraft in roll and yaw through the use of the flight control surfaces. Additionally, changes in aircraft speed were examined during the investigation. Two formation profiles were investigated; a similar formation of F-16 aircraft and a dissimilar formation of a KC-135 lead aircraft and an F-16 trail aircraft. The linear nature of the HASC95 algorithm did not account for any downward velocity in the trailing vortex. This was investigated in the flight test of a similar formation profile of F-16 aircraft.

The analytic analysis yielded a fuel savings benefit for the similar formation ranging from 16% to 34% as the aircraft was decelerated from a nominal cruise airspeed of 300 knots to maximum endurance airspeed of 210 knots. The optimal lateral position to realize these benefits remained at 13.5% wingtip overlap despite the variation in airspeed. The dissimilar formation was analyzed at a constant speed of 300 knots, which resulted in a fuel savings of 26% for the smaller trailing aircraft. The optimal lateral position resulted in a wingtip overlap of 16.7% of the F-16 wingspan. For both formations, the flight control surface deflections required to trim the aircraft were found to be within the tolerances of the F-16 control logic. This indicated that a formation autopilot to maintain the fuel savings benefit was possible. The similar formation was further analyzed during a flight test to capture the formation savings at a generalized cruise speed of 300 KCAS, maximum range airspeed of 270 KCAS, and maximum endurance airspeed of 210 KCAS.

The flight test results were inconclusive, and a direct comparison to the maximum benefit as predicted by the HASC95 analysis was not accomplished. The analysis was only accomplished for 300 KCAS due to flight test instrumentation malfunctions aboard the aircraft. The region of apparent savings, for this condition, was bounded by 7.9% to 19.9% of wingtip overlap and –3.2% to –7.3% vertically below the lead aircraft. At the boundaries, fuel savings of 13.1% and 12.1% ±7% were observed. The difference in the results was attributed to the fuel flow measurement. The flight test instrumentation system used a production fuel flow meter to record the data with a resolution of ±100 pounds per hour. For future flight test, the author recommends the use of a fuel flow measurement with a higher resolution to attain results with an uncertainty at least an order of magnitude below the expected results. The HASC95 predictions compared favorably to the flight test, however, the results were not validated.

The aircraft were manually flown while in the vortex position resulting in a high workload rating being assigned. The reason for this rating was twofold. First, the aircraft engine, in the primary operating mode, continually tuned itself for optimal performance, which affected the stabilized engine parameters. As a result, pilots were required to make constant, small throttle corrections to maintain position. For future testing of this profile in the F-16, the author recommends the use of the engine's secondary operating mode, which bypasses the self-tuning feature of the engine. This would result in stable engine parameters and decrease the workload while stabilized in the vortex position. Additionally, the relative displacement of the two aircraft was estimated during flight using visual references. This required the pilot to monitor closure and line-of-sight with respect to the lead aircraft. A real-time positional display to the pilot that provided trend information of the relative aircraft displacement could reduce the workload.

Through the analytic analyses, the dissimilar and similar formations were determined to have significant benefit over an aircraft in solo flight. The author recommends the continued research into a formation station-keeping autopilot to realize the benefit of the drag savings profile. This would altogether eliminate the workload rating from the assessment. Despite the inconclusive flight test results, it was clear that the trail aircraft flying in a vortex position off a leader aircraft would attain an increase in the range or time aloft and enhance the capability of current systems. This benefit can be attained without major modifications to existing systems.

Prior to future test of the cooperative formation profile, the author of this thesis has three recommendations. First, an improved fuel flow measurement system needs to be installed on the test aircraft that provides an uncertainty at least one order of magnitude below the expected results. Second, the engine's secondary operating mode should be used to bypass the self-tuning feature of the engine to correlate engine parameters to the test results. Finally, a real-time positional display to the pilot of the trail aircraft should be used to provide trend information of the relative aircraft displacement. Incorporating these recommendations would improve the accuracy of the flight test results and allow for the validation of the HASC95 predictive code.

Appendix A: Aircraft Schematics

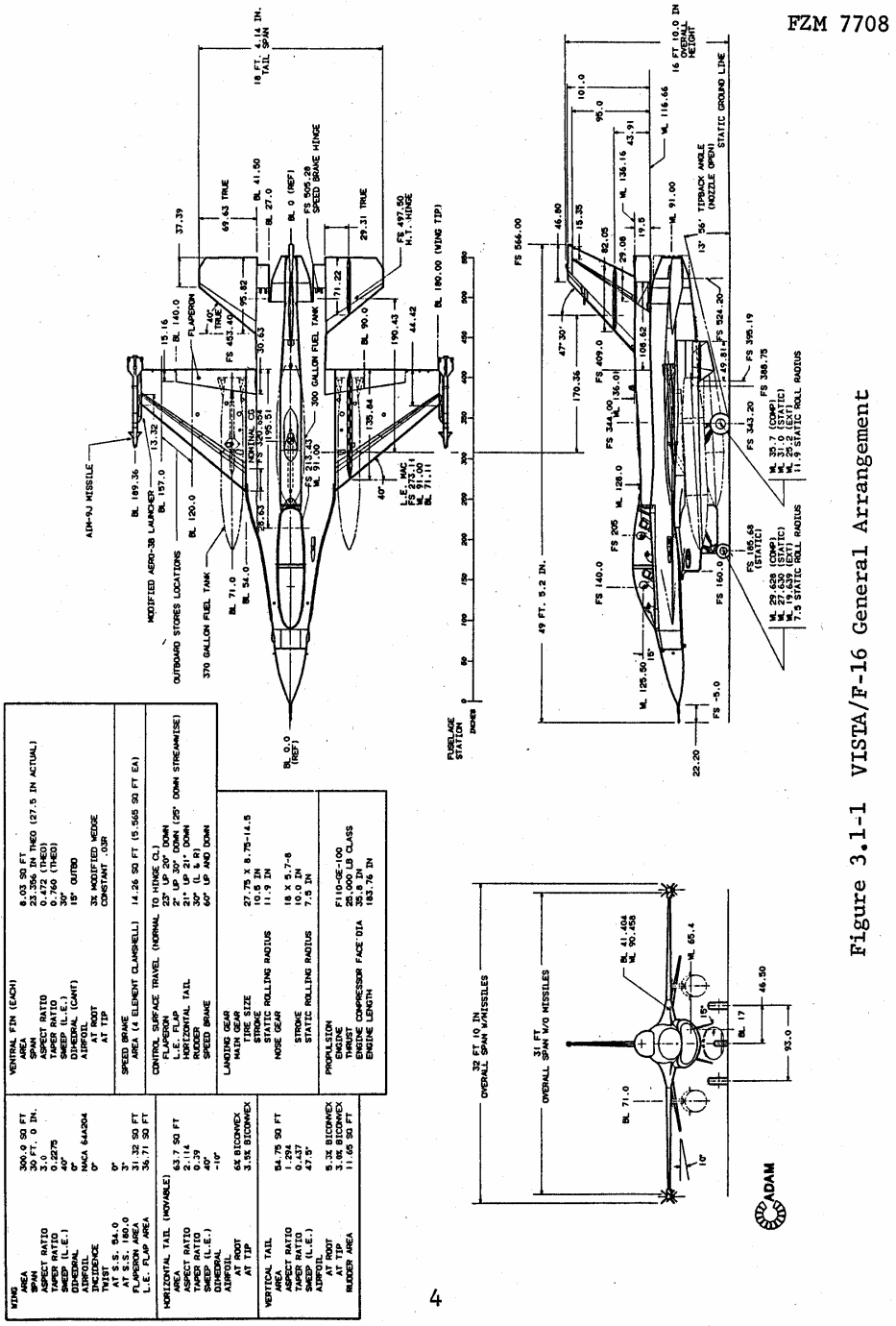

Figure 3.1-1 VISTA/F-16 General Arrangement

Figure 27. NF-16D VISTA Schematics (30:4)

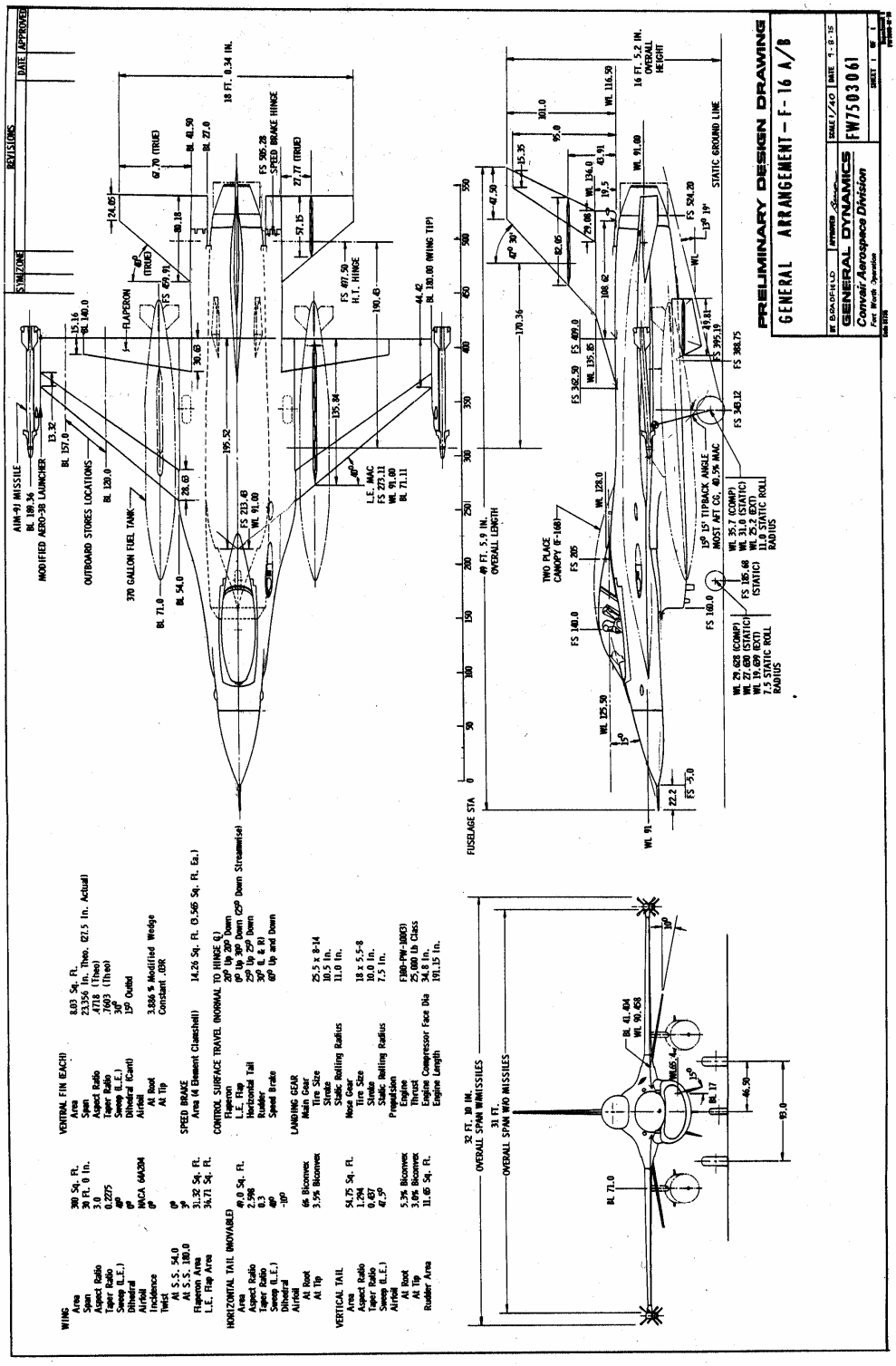

Figure 28. F-16 A/B Schematics (37:1-9)

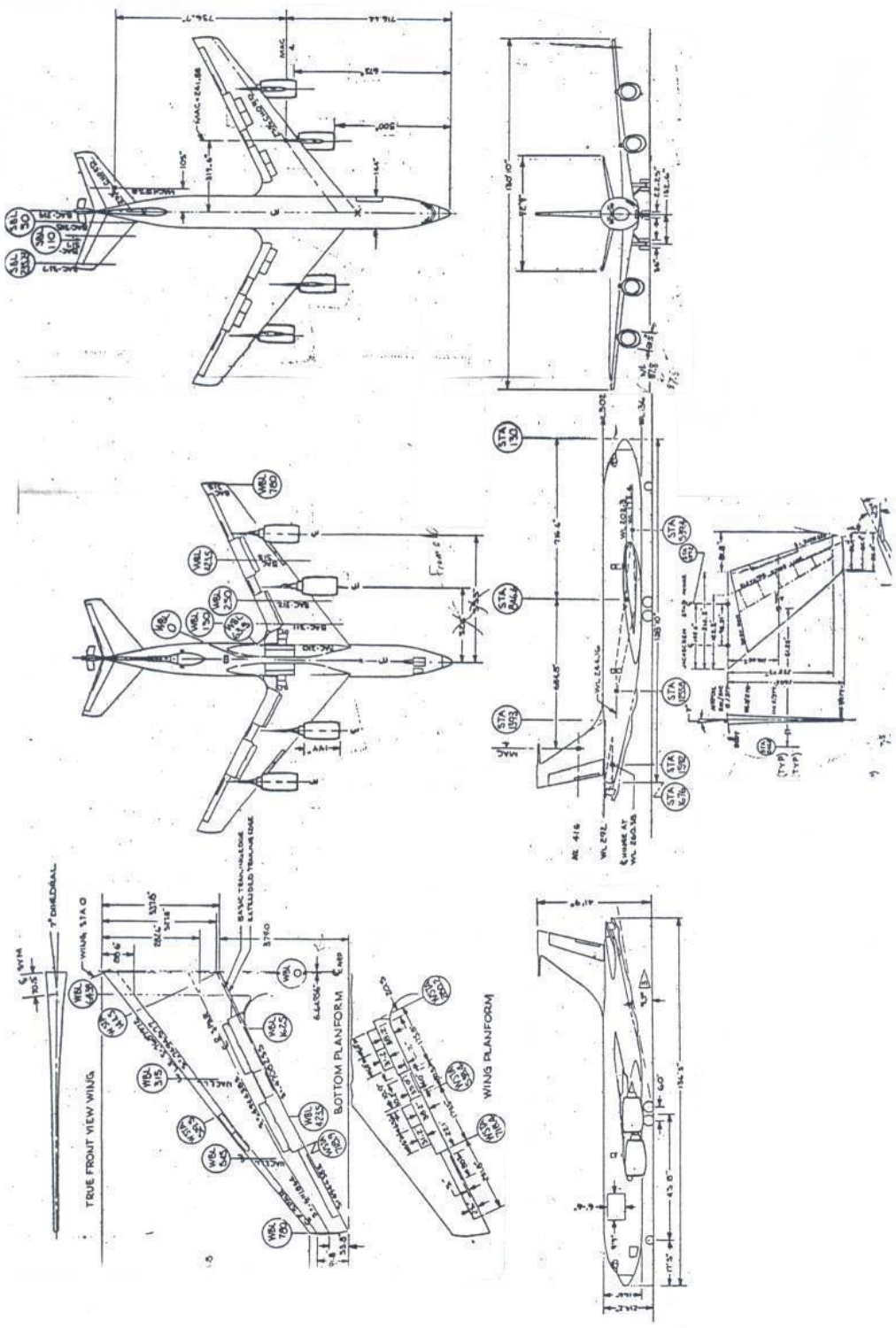

Figure 29. KC-135R Schematics (10)

Appendix B: HASC95 Input Files

B-1: Header File

This portion of the input file allows for changes in the number of panels and surfaces used in the HASC95 code. Additionally, Mach number, Reynolds Number, angle of attack and angle of sideslip are determined by this input file. The aircraft specific data, S, c, xref, zref, and wingspan are for the trail aircraft in a formation run.

```
*LAX    LAY    HAG      RUN     NPAN      NSURF     ALXP
0       1      0.       0.      52     4         0.0
*REY      NMACH(s)
20917138.75  1         0.47
*NALPHA   ALPHA(s)
03  0. 7.3 7.32
*NBETA BETA
1    0.
*PITCHQ   ROLLQ     YAWQ      V
0.        0.        0.        1.0
*SREF     CBAR      XREF      ZREF      WSPAN
43200.    135.84    320.0     0.        370.0
*******************************************************
```

B-2: NF-16D VISTA Geometrical Data

This file sets the aircraft geometry into the format required by HASC95. The file is broken into 2 surfaces; horizontal and vertical.

```
*******************************************************
HORIZONTAL
*ISRTYP   LNPAN   ISYMFLG   ENETAR   FTAIL   ALZL   XGAP
5         16         0.0      0.0     0.0    0.0        0.0
*X1       Y1        Z1        CORD1     AINC1 LEFT STAB
512.61    -110.     -12.28    37.39     0.
454.18    -40.0     0.        95.82     0.
14      8       1.0    0       0       0
*X1       Y1        Z1        CORD1     AINC1 LEFT SPEEDBRAKE FWD
213.43    -40.0      0.        328.57   0.
114.00    -30.0      0.        428.00   0.
2       18      0.0    0       0       0
*X1       Y1        Z1        CORD1     AINC1 LEFT FOREBODY
```

```
114.0     -30.0      0.       436.0     0.
60.0      -20.0      0.       490.0     0.
2       24      0.0     0       0       0
*X1       Y1        Z1        CORD1     AINC1 LEFT NOSE
60.0      -20.0      0.       490.      0.
5.0       0.0        0.       545.0     0.
4       24      0.0     0       0       0
*X1       Y1        Z1        CORD1     AINC1 LEFT WING STRAKE
253.43    -50.0      0.        126.4831 0.
213.43    -40.0      0.        164.94   0.
2       8       1.0     0       0       0
*X1       Y1        Z1        CORD1     AINC1 LEFT WING
330.9     -140.0     0.       62.93     0.
253.43    -50        0.       126.4831  0.
18      8       1.0     0       0       0
*X1       Y1        Z1        CORD1     AINC1 LEFT WING TIP
364.58    -185.0     0.       44.42     0.
330.9     -140.0     0.       78.1      0.
9       8       1.0     0       0       0
*X1       Y1        Z1        CORD1     AINC1 LEFT FLAPERON
393.84    -140.0     0.       15.16     0.
378.37    -40.00     0.       30.63     0.
20      4       0.0     0       0       0
*X1       Y1        Z1        CORD1     AINC1 RIGHT STAB
454.18    40.0     0.        95.82      0.
512.61    110.00   -12.28    37.39      0.
14      8       1.0     0       0       0
*X1       Y1        Z1        CORD1     AINC1 RIGHT SPEEDBRAKE FWD
114.00    30.0       0.        428.00   0.
213.43    40.0       0.        328.57   0.
2       18      0.0     0       0       0
*X1       Y1        Z1        CORD1     AINC1 RIGHT FOREBODY
60.0      20.0       0.       490.0     0.
114.0     30.0       0.       436.0     0.
2       24      0.0     0       0       0
*X1       Y1        Z1        CORD1     AINC1 RIGHT NOSE
5.0       0.0        0.       545.0     0.
60.0      20.0       0.       490.      0.
4       24      0.0     0       0       0
*X1       Y1        Z1        CORD1     AINC1 RIGHT WING STRAKE
213.43    40.0       0.        164.94   0.
253.43    50.0       0.        126.4831 0.
2       8       1.0     0       0       0
*X1       Y1        Z1        CORD1     AINC1 RIGHT WING
253.43    50.0       0.       126.4831  0.
330.9     140.0      0.       62.93     0.
18      8       1.0     0       0       0
*X1       Y1        Z1        CORD1     AINC1 RIGHT WING TIP
330.9     140.0      0.       78.1      0.
364.58    185.0      0.       44.42     0.
9       8       1.0     0       0       0
*X1       Y1        Z1        CORD1     AINC1 RIGHT FLAPERON OB
378.37    40.0      0.        30.63     0.
393.84    140.0      0.       15.16     0.
20      4       0.0     0       0       0
****************************
VERTICAL
*ISRTYP   LNPAN   ISYMFLG   ENETAR   FTAIL   ALZL   XGAP
5         10        0.0     0.0     0.0    0.0         0.0
*X1       Y1        Z1        CORD1     AINC1 UPPER NOSE
0.0       0.0      0.0       550.0      0.
60.0      0.0      17.5      490.0      0.
3       24      0.0     0       0       0
*X1       Y1        Z1        CORD1     AINC1 LOWER CANOPY
60.0      0.0      17.5      490.0      0.
90.0      0.0      22.5      460.0      0.
2       20      0.0     0       0       0
```

```
*X1       Y1        Z1        CORD1     AINC1 MID CANOPY
90.0      0.0      22.5      460.0      0.
125.0     0.0      45.0      425.0      0.
5       20      0.0     0       0       0
*X1       Y1        Z1        CORD1     AINC1 UPPER CANOPY
125.0     0.0      45.0      125.0      0.
160.0     0.0      55.0      5.0        0.
2       8       0.0     0       0       0
*X1       Y1        Z1        CORD1     AINC1 VERTICAL TAIL
430.0     0.0      45.0      70.0       0.
520.0     0.0      125.0     30.0       0.
16      6       1.0     0       0       0
*X1       Y1        Z1        CORD1     AINC1 RUDDER
500.0     0.0      45.0      30.0       0.
550.0     0.0      125.0     15.0       0.
16      4       0.0     0       0       0
*X1       Y1        Z1        CORD1     AINC1 LOWER NOSE
60.0      0.0      -10.0     490.0      0.
0.0       0.0      0.0       550.0      0.
2       24      0.0     0       0       0
*X1       Y1        Z1        CORD1     AINC1 NACELLE
160.0     0.0      -30.0     290.0      0.
160.0     0.0      -10.0     390.0      0.
4       18      0.0     0       0       0
*X1       Y1        Z1        CORD1     AINC1 LEFT FIN
405.0     -25.0      -15.0     40.0      0.
395.0     -15.0        0.0     50.0      0.
2       6       1.0     0       0       0
*X1       Y1        Z1        CORD1     AINC1 RIGHT FIN
395.0     15.0        0.0     50.0      0.
405.0     25.0     -15.0     40.0       0.
2       6       1.0     0       0       0
*********************************************************
```

B-3: F-16B Geometrical Data

```
*********************************************************
HORIZONTAL
*ISRTYP   LNPAN   ISYMFLG   ENETAR   FTAIL   ALZL   XGAP
5         16         0.0      0.0     0.0    0.0         0.0
*X1       Y1        Z1        CORD1     AINC1 LEFT STAB
515.00    -105.     -11.93    25.00      0.
460.00    -40.0     0.        80.00      0.
13      8       1.0     0       0       0
*X1       Y1        Z1        CORD1     AINC1 LEFT SPEEDBRAKE FWD
213.43    -40.0      0.        328.57    0.
114.00    -30.0      0.        428.00    0.
2       18      0.0     0       0       0
*X1       Y1        Z1        CORD1     AINC1 LEFT FOREBODY
114.0     -30.0      0.        436.0     0.
60.0      -20.0      0.        490.0     0.
2       24      0.0     0       0       0
*X1       Y1        Z1        CORD1     AINC1 LEFT NOSE
60.0      -20.0      0.        490.      0.
5.0       0.0        0.        545.0     0.
4       24      0.0     0       0       0
*X1       Y1        Z1        CORD1     AINC1 LEFT WING STRAKE
253.43    -50.0      0.        126.48    0.
213.43    -40.0      0.        164.94    0.
2       8       1.0     0       0       0
```

```
*X1       Y1        Z1        CORD1     AINC1 LEFT WING
330.9     -140.0     0.       62.93     0.
253.43    -50        0.       126.48    0.
18      8       1.0    0       0       0
*X1       Y1        Z1        CORD1     AINC1 LEFT WING TIP
364.58    -185.0     0.       44.42     0.
330.9     -140.0     0.       78.1      0.
9       8       1.0    0       0       0
*X1       Y1        Z1        CORD1     AINC1 LEFT FLAPERON
393.84    -140.0     0.       15.16     0.
378.37    -40.00     0.       30.63     0.
20      4       0.0    0       0       0
*X1       Y1        Z1        CORD1     AINC1 RIGHT STAB
460.00    40.0     0.        80.00     0.
515.00    105.     -11.93    25.00     0.
13      8       1.0    0       0       0
*X1       Y1        Z1        CORD1     AINC1 RIGHT SPEEDBRAKE FWD
114.00    30.0       0.        428.00   0.
213.43    40.0       0.        328.57   0.
2       18      0.0    0       0       0
*X1       Y1        Z1        CORD1     AINC1 RIGHT FOREBODY
60.0      20.0       0.       490.0     0.
114.0     30.0       0.       436.0     0.
2       24      0.0    0       0       0
*X1       Y1        Z1        CORD1     AINC1 RIGHT NOSE
5.0       0.0        0.       545.0     0.
60.0      20.0       0.       490.      0.
4       24      0.0    0       0       0
*X1       Y1        Z1        CORD1     AINC1 RIGHT WING STRAKE
213.43    40.0       0.        164.94   0.
253.43    50.0       0.        126.48   0.
2       8       1.0    0       0       0
*X1       Y1        Z1        CORD1     AINC1 RIGHT WING
253.43    50.0       0.       126.48    0.
330.9     140.0      0.       62.93     0.
18      8       1.0    0       0       0
*X1       Y1        Z1        CORD1     AINC1 RIGHT WING TIP
330.9     140.0      0.       78.1      0.
364.58    185.0      0.       44.42     0.
9       8       1.0    0       0       0
*X1       Y1        Z1        CORD1     AINC1 RIGHT FLAPERON OB
378.37    40.0      0.        30.63     0.
393.84    140.0      0.       15.16     0.
20      4       0.0    0       0       0
****************************
VERTICAL
*ISRTYP   LNPAN   ISYMFLG   ENETAR   FTAIL   ALZL   XGAP
5         10        0.0      0.0     0.0    0.0         0.0
*X1       Y1        Z1        CORD1     AINC1 UPPER NOSE
0.0       0.0      0.0       550.0     0.
80.0      0.0      15.5      470.0     0.
3       24      0.0    0       0       0
*X1       Y1        Z1        CORD1     AINC1 LOWER CANOPY
80.0      0.0      15.5      470.0     0.
105.0     0.0      25.5      445.0     0.
2       20      0.0    0       0       0
*X1       Y1        Z1        CORD1     AINC1 UPPER CANOPY
105.0     0.0      25.5      160.0     0.
170.0     0.0      45.0        5.0     0.
5       8       0.0    0       0       0
*X1       Y1        Z1        CORD1     AINC1 LOWER TAIL
362.5     0.0      25.5      167.5     0.
430.0     0.0      45.0      100.0     0.
2       12      0.0    0       0       0
*X1       Y1        Z1        CORD1     AINC1 VERTICAL TAIL
430.0     0.0      45.0      70.0      0.
520.0     0.0      125.0     30.0      0.
```

```
16      6       1.0     0       0       0
*X1       Y1         Z1         CORD1     AINC1 RUDDER
500.0     0.0       45.0       30.0       0.
550.0     0.0       125.0      15.0       0.
16      4       0.0     0       0       0
*X1       Y1         Z1         CORD1     AINC1 LOWER NOSE
60.0      0.0       -10.0      490.0      0.
0.0       0.0       0.0        550.0      0.
2       24      0.0     0       0       0
*X1       Y1         Z1         CORD1     AINC1 NACELLE
160.0     0.0       -30.0      290.0      0.
160.0     0.0       -10.0      390.0      0.
4       18      0.0     0       0       0
*X1       Y1         Z1         CORD1     AINC1 LEFT FIN
405.0     -25.0      -15.0       40.0      0.
395.0     -15.0        0.0       50.0      0.
2       6       1.0     0       0       0
*X1       Y1         Z1         CORD1     AINC1 RIGHT FIN
395.0     15.0         0.0      50.0      0.
405.0     25.0       -15.0      40.0      0.
2       6       1.0     0       0       0
*****************************************
```

B-4: KC-135R Geometrical Data

```
1658.2    -255.0    289.45      87.8      -5.7
1450.0       0.0    258.14     214.2      -5.7
 17.        10.       1.         00        00        0.0
*********************************************************
1450.0       0.0    258.14     214.2      -5.7
1658.2     255.0    289.45      87.8      -5.7
 17.        10.       1.         00        00        0.0
*********************************************************
360.0        0.0    136.0      700.0     0.0
188.0        0.0    175.0     1182.0     0.0
  4.        40.       0.         00        00        0.0
*********************************************************
188.0        0.0    175.0     1182.0     0.0
130.0        0.0    208.0     1377.0     0.0
  3.        40.       0.         00        00        0.0
*********************************************************
130.0        0.0    208.0     1377.0     0.0
220.0        0.0    258.0     1456.0     0.0
  4.        40.       0.         00        00        0.0
*********************************************************
220.0        0.0    258.0     1456.0     0.0
360.0        0.0    302.0     1316.0     0.0
  4.        40.       0.         00        00        0.0
*********************************************************
1393.0       0.0    302.0      242.0     0.0
1580.0       0.0    558.6      109.0     0.0
 12.        10.       1.         00        00        0.0
*********************************************************
1180.7    -780.0    270.77     112.0     2.0
580.0        0.0    175.0      334.3     2.0
 52.        10.       1.         00        00        0.0
*********************************************************
580.0        0.0    175.0      334.3     2.0
1180.7     780.0    270.77     112.0     2.0
 52.        10.       1.         00        00        0.0
*********************************************************
```

Appendix C: Supplemental Graphs

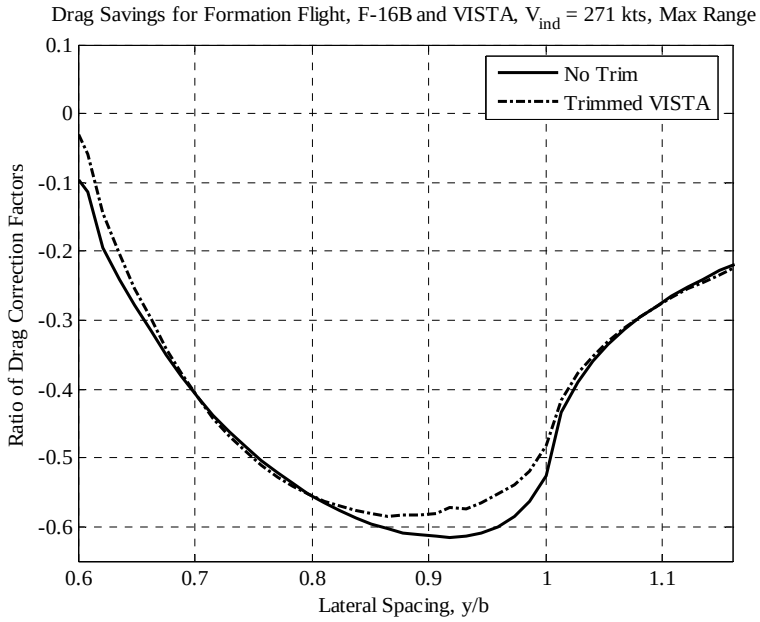

Figure 30. Trimmed Drag Reduction, Maximum Range

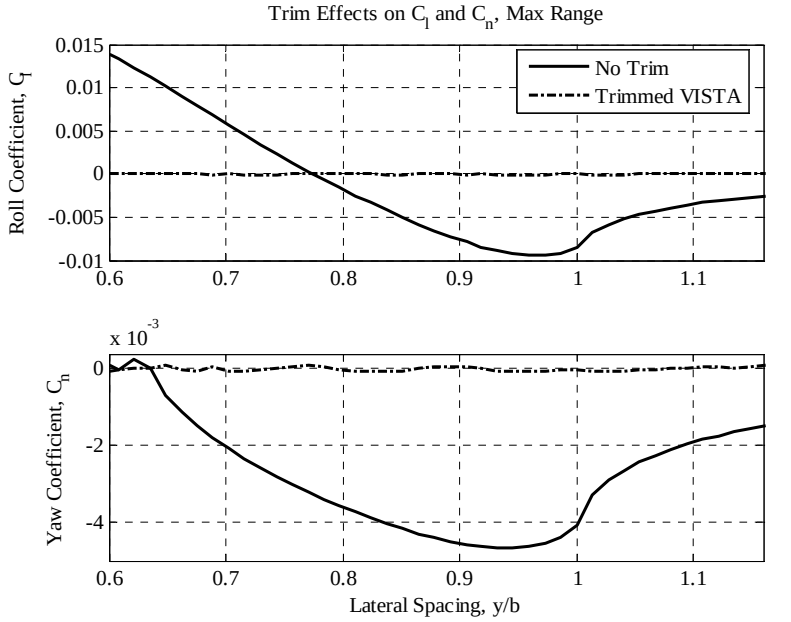

Figure 31. Trimmed C_l and C_n, Maximum Range

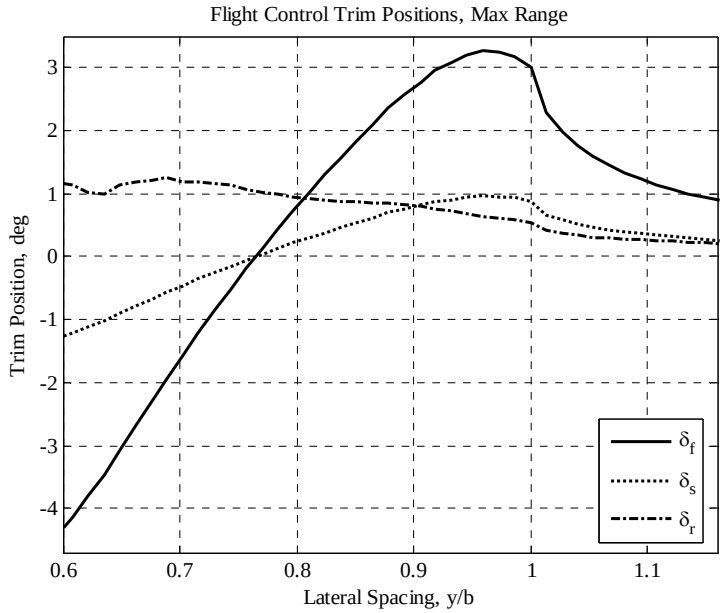

Figure 32. Flight Control Trim Positions, Maximum Range

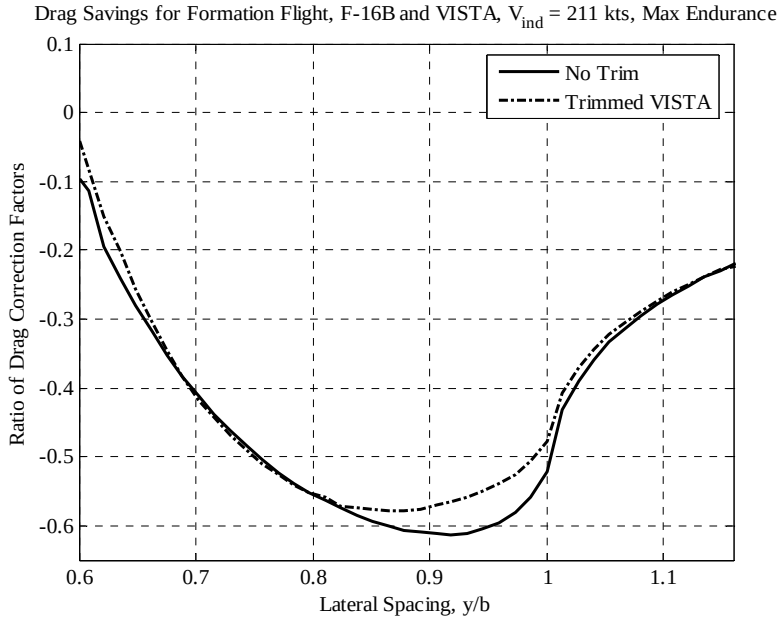

Figure 33. Trimmed Drag Reduction, Maximum Endurance

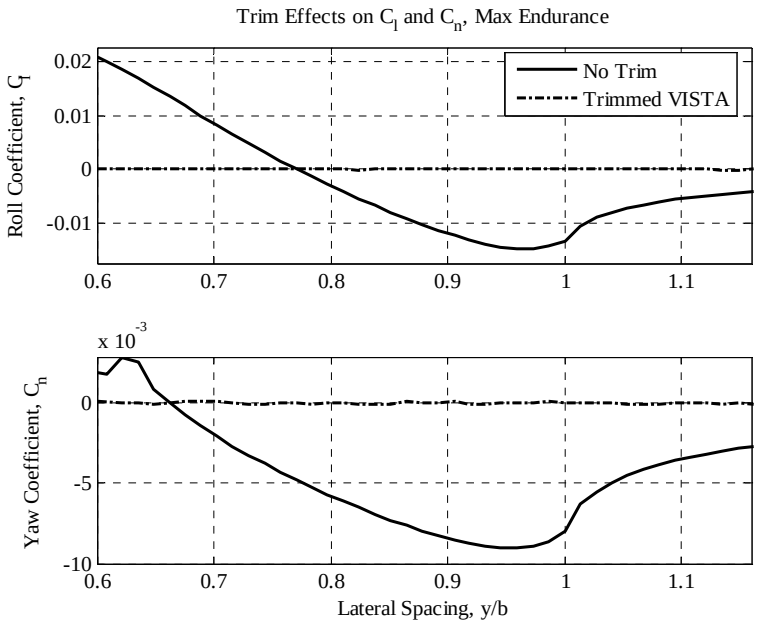

Figure 34. Trimmed C_l and C_n, Maximum Endurance

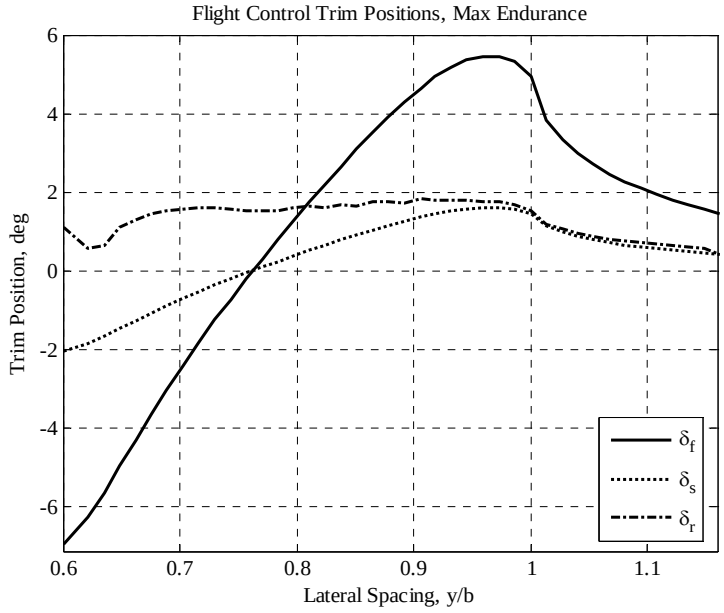

Figure 35. Flight Control Trim Positions, Maximum Endurance

Appendix D: Supplemental Computer Code

D-1 Mice.f

The following code was developed by Mr. Blake, AFRL (7) to account for the movement of the lead aircraft in the simulation. It is designed to be used in conjunction with the HASC95 program. Both representations, similar and dissimilar formations are represented within the code.

```
      program move
c
c  this code shifts the coordinates of a
c  HASC95 input file to simulate a formation of
c  aircraft by defining new aircraft positions
c
c  file "header" is the hasc header + receiver input
c  file "kc135" is the kc135 geometry
c  file "ftemp" is the aerodynamic result file from hasc
c  file "hasc.inp" is the generated hasc input file
c
c  +x = lead vehicle upstream
c  +y = lead vehicle right
c  +z = lead vehicle below
c
      character*80 f1
c
      open(90,file='trail.txt',status='old')
c       open(91,file='lead.txt',status='old')
                open(91,file='kc135.txt',status='old')
      open(92,file='ftemp.txt',status='unknown')
                open(102,file='final.txt',status='unknown')
c
      alpl=0.
c               span=370.
      span=1560.
c
c  loop on relative aircraft x,y,z positions
c
c       delx=2.0*span
c      delz=0.
                delx=1856.
                delz=202.0
      do 1000 iy=75,125
      dely=10.*(iy-1)
         open(15,file='hasc.inp',status='unknown')
c
c  write header + Receiver aircraft to hasc input file
c
            do 3100 ii=1,130
              read(90,900) f1
```

```
              write(15,900) f1
 3100         continue
c
c     rewind header+Receiver for next case
c
            rewind(90)
c
c  write F-16B leader to hasc input file
c
c            do 3400 ij=1,16
c               read(91,900) f1
c               write(15,900) f1
c               read(91,*) x1,y1,z1,c1,a1
c               write(15,910) x1-delx,y1+dely,z1-delz,c1,a1+alpl
c               read(91,*) x1,y1,z1,c1,a1
c               write(15,910) x1-delx,y1+dely,z1-delz,c1,a1+alpl
c               read(91,900) f1
c               write(15,900) f1
c 3400         continue
c               read(91,900) f1
c               write(15,900) f1
c               read(91,900) f1
c               write(15,900) f1
c               read(91,900) f1
c               write(15,900) f1
c               read(91,900) f1
c               write(15,900) f1
c            do 3450 ik=1,10
c               read(91,900) f1
c               write(15,900) f1
c               read(91,*) x1,y1,z1,c1,a1
c               write(15,910) x1-delx,y1+dely,z1-delz,c1,a1+alpl
c               read(91,*) x1,y1,z1,c1,a1
c               write(15,910) x1-delx,y1+dely,z1-delz,c1,a1+alpl
c               read(91,900) f1
c               write(15,900) f1
c 3450         continue
c
c     write KC-135 leader to hasc input file
c
            do 3400 ij=1,9
               read(91,*) x1,y1,z1,c1,a1
               write(15,910) x1-delx,y1+dely,z1-delz,c1,a1+alpl
               read(91,*) x1,y1,z1,c1,a1
               write(15,910) x1-delx,y1+dely,z1-delz,c1,a1+alpl
               read(91,900) f1
               write(15,900) f1
               read(91,900) f1
               write(15,900) f1
 3400         continue
c
c     rewind wing geometry file for next case
c
            rewind(91)
c
c     rewind input file for hasc run
c
            rewind(15)
c
c     rewind aero file so it can be written
c
            rewind(92)
c
c     run hasc
c
            call hasc
```

```
c
c     rewind aero file written by hasc so it can be read
c
           rewind(92)
           read(92,*) aoa,cl1,cl2,cd2,cm2,cy2,cll2,cln2
c
c     compute increments for sim table look-up
c
c          dcy2=cy2-cy2s
c          dcll2=cll2-cll2s
c          dcln2=cln2-cln2s
c
c  print output files
c
        write(102,925) (delx-130.)/span,dely/span,(delz-202.)/span,
     1        aoa,cl1,cl2,cd2,cm2,cy2,cll2,cln2
c
           rewind(15)
c
 1000 continue
c
  900 format(a80)
  910 format(5(f9.2,1x))
  920 format(1x,1f8.3,7f9.4)
  925 format(1x,3f7.3,8f9.5)
      close(90,status='keep')
      close(91,status='keep')
      close(92,status='keep')
              close(93,status='keep')
      stop
      end
```

D-2: Printemp.f

This subroutine was designed by Mr. Blake (7). It is to be used in conjunction with the basic HASC95 code and the movement subroutine, D-1. The subroutine extrapolates the aerodynamic coefficients for the trail aircraft in the formation.

```
      subroutine pritot

c...purpose:
c   print total forces and moments in body axes,
c   wind axes, and stability axes.

c...output:  unit 75 (hasc.out)

c...subroutine called by hasc
c   subroutine calls:  none

c...discussion:  this is adapted from basic vorlax print routines.
c   the forces and moments are initially in body axis
c   they are translated to wind and stability axis and
c   printed out as a summary for each axis. in this routine
c   only total forces are printed.
```

```
      parameter (lun=201, ntal=30)

      include 'flowopts.cmn'
      include 'set3.cmn'
      include 'set5.cmn'
      include 'set6.cmn'
      include 'set8.cmn'
      include 'set9.cmn'
      include 'set11.cmn'
      include 'set12.cmn'
      include 'set13.cmn'
      include 'set14.cmn'
      include 'set15.cmn'
      include 'set17.cmn'
      include 'set21.cmn'
      include 'set23.cmn'
      include 'set24.cmn'

      include 'print.cmn'
      include 'forces.cmn'
      include 'srffrc.cmn'
      include 'version.cmn'

      pi  = 4.0 * atan(1.0)
      dtr = pi / 180.

c...print heading with hasc version and release date

      write(75,1104) vtitle
1104  format(1x,a55)
      write(75,1114)
1114  format(1x,'** Total Force and Moments **')

c...printout total configuration data .

      write(75,105) jobtitl
 105  format(1x,a)

      write(75,120) mach(iq), -yawstb(ib),
     & pitchq,-rollq,-yawq,vinf
 120  format(1x,'Mach = ',f6.2,/,1x,'Beta = ',f6.2,/,
     & 1x,'Pitch rate(/sec) =',f7.2,/,
     & 1x,'Roll rate(/sec)  =',f7.2,/,
     & 1x,'Yaw rate(/sec)   =',f7.2,/,
     & 1x,'Vinf       =',f10.2)

      write(75,6662) sref,wspan,cbar
6662  format(/,1x,'Sref = ',f9.3,'  Wspan = ',f9.3,'  Cbar = ',f9.3)
      write(75,6663) xbar, zbar
6663  format(1x,'Xbar = ',f9.3,'  Zbar  = ',f9.3)

      write(75,190)
 190  format (/,' ************  BODY AXIS SYSTEM  ***************')

      write(75,7503)
7503  format(1x,'All Surfaces Body Axis')

 300  write(75,310)
 310  format(1x,'  Alpha     Beta    CNtot    CAtot    Cmtot  ',
     &         '  CYtot   Cltot    Cntot')

c...unit 73 for tecplot input file

      write(73,7315) jobtitl
7315  format('TITLE=',"",a,"")
```

```
      write(73,7317)
7317  format('VARIABLES=ALPHA,BETA,CN,CA,CM,CY,CLLB,CLN,CL,CD')

      write(73,7316)  mach(iq), -yawstb(ib)
7316  format('ZONE T="'Totals',' M=',f5.2,' Beta=',f6.2,'", F=POINT')

      do 600 ihh = 1,nalpha
        write(75,320) alfstb(ihh), -yawstb(ib), acztot(ihh),
     &  acxtot(ihh), amytot(ihh)/cbar, acytot(ihh), amxtot(ihh)/wspan,
     &  amztot(ihh)/wspan
 320    format(1x,2f8.3,6f9.4)

c...unit 73 for tecplot input
          astb   = alfstb(ihh)
          sinast = sin(dtr*astb)
          cosast = cos(dtr*astb)
          cltemp = -sinast*acxtot(ihh) + cosast*acztot(ihh)
          cdtemp =  cosast*acxtot(ihh) + sinast*acztot(ihh)
        write(73,322) alfstb(ihh), -yawstb(ib), acztot(ihh),
     &  acxtot(ihh), amytot(ihh)/cbar, acytot(ihh), amxtot(ihh)/wspan,
     &  amztot(ihh)/wspan,cltemp,cdtemp
 322    format(1x,2f6.2,6f9.4,2f11.6)
7332    format(1x,2f8.3,6f9.4)

600   continue
      if (wspan.gt.0.) go to 666

      write(75,290)
 290  format (/,' ************  WIND AXIS SYSTEM  **************')

      write(75,7504)
7504  format(1x,'All Surfaces Wind Axis')

      write(75,410)
 410  format(1x,'  Alpha     Beta    CLtot    CDtot    Cmtot ',
     &          '   CYtot    Crtot    Cntot')

      do 601 ihh = 1,nalpha

        astb = alfstb(ihh)

c...yawstb multiplied by -1 to give betstb
        sinast = sin (dtr*astb)
        sinbst = sin (dtr*(-yawstb(ib)))
        cosast = cos (dtr*astb)
        cosbst = cos (dtr*(-yawstb(ib)))

c...transform panel forces to wind axes

        cltotw = -sinast*acxtot(ihh) + cosast*acztot(ihh)

        cdtotw = cosbst*cosast*acxtot(ihh)  - sinbst*acytot(ihh)
     &         + cosbst*sinast*acztot(ihh)

        cytotw = -sinbst*cosast*acxtot(ihh) + cosbst*acytot(ihh)
     &           -sinbst*sinast*acztot(ihh)

        cmtotw = -sinbst*cosast*amxtot(ihh) + cosbst*amytot(ihh)
     &           -sinbst*sinast*amztot(ihh)

        crtotw =  cosbst*cosast*amxtot(ihh) + sinbst*amytot(ihh)
     &           +cosbst*sinast*amztot(ihh)

        cntotw = -sinast*amxtot(ihh) + cosast*amztot(ihh)

        cmtotw = cmtotw / cbar
```

```
      crtotw = crtotw / wspan
      cntotw = cntotw / wspan

      write(75,320) alfstb(ihh), -yawstb(ib), cltotw, cdtotw,
     &  cmtotw, cytotw, crtotw, cntotw

 601  continue
 666  continue

     write(75,490)
 490  format (/,' ************  STABILITY AXIS SYSTEM  ************')

     write(75,7505)
7505  format(1x,'All Surfaces Stab Axis')


     write(75,510)
 510  format(1x,'  Alpha     Beta    CLtot    CDtot    Cmtot ',
     &         ' CYtot    Cltot    Cntot')
     write(6,6611)
6611  format(/,' Total Stability Axis Data ')
     write(6,6612)
6612  format('   Alpha    Beta      CL       CD       Cm       Cy',
     &'       Cl',
     &       '       Cn')

     do 602 ihh = 1,nalpha

       astb   = alfstb(ihh)
       sinast = sin(dtr*astb)
       cosast = cos(dtr*astb)

c...transfer total forces and moments to stability axis

       cltots = -sinast*acxtot(ihh) + cosast*acztot(ihh)
       cdtots =  cosast*acxtot(ihh) + sinast*acztot(ihh)
       cytots =  acytot(ihh)
       cmtots =  amytot(ihh)
       crtots =  cosast*amxtot(ihh) + sinast*amztot(ihh)
       cntots = -sinast*amxtot(ihh) + cosast*amztot(ihh)
       cmtots =  cmtots / cbar
       crtots =  crtots / wspan
       cntots =  cntots / wspan

       write(75,320)  alfstb(ihh),-yawstb(ib), cltots, cdtots,
     &  cmtots, cytots, crtots, cntots

     write(6,6680) alfstb(ihh),-yawstb(ib),cltots, cdtots,
     & cmtots, cytots, crtots, cntots
6680  format(2F8.3,6F9.4)

602    continue
c
c  temporary code for VISTA F-16 calculations
c
     do 8000 j=1,nalpha
c      cntemp=acztot(j)-scztot(3,j)-scztot(4,j)
c      catemp=acxtot(j)-scxtot(3,j)-scxtot(4,j)
c      cytemp=acytot(j)-scytot(3,j)-scytot(4,j)
c      cmtemp=amytot(j)/cbar-(scqtot(3,j)+scqtot(4,j))/cbar
c      clntemp=amztot(j)/wspan-(scrtot(3,j)+scrtot(4,j))/wspan
c      clltemp=amxtot(j)/wspan-(scptot(3,j)+scptot(4,j))/wspan
c
c      cltemp=cntemp*cos(dtr*alfstb(j))-catemp*sin(dtr*alfstb(j))
c      cdtemp=catemp*cos(dtr*alfstb(j))+cntemp*sin(dtr*alfstb(j))
c      cl2=(scztot(3,j)+scztot(4,j))*cos(dtr*alfstb(j))
```

```
c     1   -(scxtot(3,j)+scztot(4,j))*sin(dtr*alfstb(j))
      cntemp=acztot(j)-scztot(3,j)
      catemp=acxtot(j)-scxtot(3,j)
      cytemp=acytot(j)-scytot(3,j)
      cmtemp=amytot(j)/cbar-(scqtot(3,j))/cbar
      clntemp=amztot(j)/wspan-(scrtot(3,j))/wspan
      clltemp=amxtot(j)/wspan-(scptot(3,j))/wspan
c
      cltemp=cntemp*cos(dtr*alfstb(j))-catemp*sin(dtr*alfstb(j))
      cdtemp=catemp*cos(dtr*alfstb(j))+cntemp*sin(dtr*alfstb(j))
      cl2=(scztot(3,j))*cos(dtr*alfstb(j))
     1   -(scxtot(3,j))*sin(dtr*alfstb(j))
      if(j.eq.nalpha)  write(92,8100) alfstb(j),
     1             cl2,cltemp,cdtemp,cmtemp,
     2             cytemp,clltemp,clntemp
 8000 continue
 8100 format(f6.2,7f10.5)

      return
      end
```

Appendix E: Data Acquisition System Parameters

Table 9. F-16 Data Acquisition System Parameters (32:6-14-6-15)

Parameter	Source	Range	Resolution	Sample Rate (Hz)
Left Flaperon Position	Analog	± 20º	0.02º	66.67
Right Flaperon Position	Analog	± 20º	0.02º	66.67
Left Horizontal Tail Position	Analog	± 25º	0.03º	66.67
Right Horizontal Tail Position	Analog	± 25º	0.03º	66.67
Rudder Position	Analog	± 30º	0.03º	66.67
Total Fuel Flow	Analog	1100 to 80100 lbs/hr	20 lbs/hr	8.33
Power Lever Angle	Analog	16.5º to 130º	0.06º	8.33
Core Speed N2	Analog	5 to 110% rpm	0.01% rpm	8.33
Pressure Altitude	Digital - 16 Bit	-1500 to 60,000 ft MSL	1 ft	8.33
Heading Angle	Digital - 14 Bit	± 180º	0.03º	66.67
Pitch Angle	Digital - 14 Bit	± 90º	0.02º	66.67
Roll Angle	Digital - 14 Bit	± 180º	0.03º	66.67
Mach Number	Digital - 16 Bit	0.1 to 3.0	0.0003	8.33
True Airspeed	Digital - 15 Bit	70 to 1700 kt	0.13 kt	8.33
Calibrated Airspeed	Digital - 15 Bit	50 to 1000 kt	0.07 kt	8.33
Total Fuel Weight	Analog	0 to 5100 lbs	11 lbs	8.33
Total Air Temperature	Digital	-100º to 250º F	0.09º F	8.33
Event Marker	Discrete		Discrete	66.67
IRIG Time				66.67
Note: Measurement Uncertainty was five times the data resolution				

Appendix F: Workload Assessment Scale

Table 10. 7-Point Workload Scale (2:3)

Rating	Definition
1	Nothing to do; No system demands
2	Light Activity; Minimum system demands
3	Moderate Activity; Easily managed; Considerable Spare Time
4	Busy; Challenging but manageable; Adequate time available
5	Very Busy; Demanding to manage; Barely enough time
6	Extremely Busy; Very difficult; Nonessential tasks postponed
7	Overloaded; System unmanageable; Essential tasks undone; Unsafe

Appendix G: Flight Test Results

Table 11. Test Day Conditions, Mission 1

Test Run Number	Position*	h_{ic} (feet)	V_{CAL} (KCAS)	T_{static} (°F)	Gross Weight (pounds)	Energy Height Approximation ($E_s=At^2+Bt+C$, feet)		
						A	B	C
1	VOR	19980	299	8.58	24320	-0.083148	0.550040	27391.5
	SS	20020	300	9.30	24310	0.035234	-0.141240	27475.8
2	VOR	19980	301	9.13	24290	-0.067109	3.137770	27433.9
	SS	19970	302	9.10	24260	-0.050214	-0.032410	27510.7
3	VOR	19980	298	12.05	24250	0.124044	-2.310600	27293.4
4	VOR	19980	298	8.30	24210	0.153004	1.261610	27233.1
5	VOR	19970	300	8.62	24020	0.015070	-0.895269	27438.5
	SS	19950	300	9.19	23890	0.131094	-8.163273	27461.8
6	VOR	19960	299	8.44	23740	0.026537	-3.052454	27397.3
7	VOR	19960	300	8.64	23490	0.011749	-1.033675	27410.7
8	VOR	19980	298	8.18	24220	0.104216	-7.114520	27406.6
* VOR: In Vortex, SS: Single Ship at Test Airspeed								

Table 12. Test Day Conditions, Mission 3

Test Run Number	Position*	h_{ic} (feet)	V_{CAL} (KCAS)	T_{static} (°F)	Gross Weight (pounds)	Energy Height Approximation ($E_s=At^2+Bt+C$, feet)		
						A	B	C
1	VOR	19720	308	0.78	24210	0.006232	1.861726	27123.8
	SS	19910	309	0.89	24170	0.157734	-5.079938	27495.7
2	VOR	19960	300	-0.53	24040	0.080829	-6.169410	27220.0
	SS	19850	300	-0.44	24050	0.041996	-0.011557	26974.5
3	VOR	19940	303	-0.04	24020	0.018895	0.558633	27242.2
	SS	19850	304	0.26	23990	0.083660	-7.154364	27310.3
4	VOR	19910	304	-0.05	23960	-0.007335	-0.610575	27278.8
	SS	19830	305	3.97	23880	0.262622	-9.028383	27231.8
5	VOR	19820	295	-0.77	23790	-0.113529	3.727326	26774.4
	SS	19760	296	-0.46	23760	0.108008	-9.095350	26892.9
6	VOR	19920	302	0.03	23960	0.013704	0.090215	27191.0
* VOR: In Vortex, SS: Single Ship at Test Airspeed								

Table 13. 300 KCAS Flight Test Results, Fuel Savings Analysis

Mission	Test Run Number	x/b (std dev)	Wingtip Overlap (y/b) (std dev)	z/b (std dev)	Fuel Savings (%)	ΔV_{CAL} (KCAS)	ΔRPM (%)
1	1	2.21 (0.03)	0.09 (0.01)	-0.03 (0.01)	6.8	15.8	1.1
	2	2.17 (0.01)	0.14 (0.01)	-0.01 (0.01)	6.7	43.9	1.5
	3	2.27 (0.02)	0.08 (0.02)	-0.03 (0.01)	13.1	25.3	1.2
	4	2.26 (0.02)	0.06 (0.03)	-0.03 (0.01)	1.6	18.7	1.2
	5	2.24 (0.04)	0.03 (0.01)	-0.11 (0.01)	0.2	7.3	0.4
	6	2.33 (0.01)	0.16 (0.01)	-0.06 (0.01)	5.3	0.8	0.4
	7	2.13 (0.04)	0.01 (0.01)	-0.16 (0.01)	1.5	21.3	1.1
	8	2.18 (0.03)	0.02 (0.01)	-0.04 (0.01)	0.1	0.0	0.8
3	1	2.03 (0.02)	0.22 (0.02)	0.004 (0.02)	0.4	5.7	0.5
	2	2.10 (0.03)	0.15 (0.02)	0.003 (0.01)	7.1	10.7	0.9
	3	2.10 (0.03)	0.20 (0.02)	-0.07 (0.01)	12.1	13.1	1.2
	4	2.01 (0.03)	0.09 (0.01)	-0.06 (0.01)	1.0	17.1	1.3
	5	2.20 (0.06)	0.03 (0.03)	-0.09 (0.02)	0.9	14.7	0.5
	6	2.03 (0.05)	0.01 (0.01)	-0.09 (0.01)	3.7	0.0	0.9

Table 14. 300 KCAS Flight Test Results, Control Surface Determination

Mission	Test Run Number	$\delta_{r\,\text{resultant}}$ (deg)	$\delta_{s\text{resultant}}$ (deg)	$\delta_{f\,\text{resultant}}$ (deg)
1	1	0.4	0.5	1.7
	2	0.4	0.5	1.7
	3	0.4	0.5	1.7
	4	0.2	0.2	0.8
	5	0.3	0.2	1.0
	6	0.2	0.1	0.6
	7	0.2	0.2	0.8
	8	0.3	0.3	1.2
3	1	0.4	0.5	1.9
	2	0.2	0.3	1.1
	3	0.3	0.5	1.8
	4	0.3	0.5	1.7
	5	0.3	0.6	2.0
	6	0.2	0.3	1.0

Table 15. 300 KCAS Flight Test Results, Pilot Workload

Mission	Test Run Number	Workload Rating
1	1	5
	2	5
	3	6
	4	5
	5	5
	6	6
	7	6
	8	4
3	1	4
	2	5
	3	5
	4	3
	5	3
	6	4

Table 16. 270 KCAS Flight Test Estimations

Mission	Test Run Number	x/b (std dev)	Wingtip Overlap (y/b) (std dev)	z/b (std dev)	Fuel Savings (%)	Workload Rating
4	1	2.16 (0.05)	-0.002 (0.02)	-0.04 (0.01)	8.5	5
	2	2.19 (0.02)	0.11 (0.01)	0.02 (0.01)	16.7	5
	3	2.19 (0.03)	0.10 (0.01)	-0.02 (0.01)	-1.8	6
	4	2.22 (0.04)	0.02 (0.01)	-0.04 (0.01)	-1.9	5
	5	2.24 (0.05)	0.10 (0.01)	-0.06 (0.01)	15.8	5
	6	2.19 (0.05)	0.16 (0.02)	-0.03 (0.01)	8.9	6
	7	2.06 (0.06)	-0.01 (0.03)	-0.06 (0.01)	0.0	4
	8	2.16 (0.03)	-0.01 (0.01)	-0.02 (0.01)	-3.7	4

Table 17. 210 KCAS Flight Test Estimations

Mission	Test Run Number	x/b (std dev)	Wingtip Overlap (y/b) (std dev)	z/b (std dev)	Fuel Savings (%)	Workload Rating
5	1	2.44 (0.07)	0.05 (0.02)	0.05 (0.01)	11.1	5
	2	2.01 (0.04)	0.14 (0.01)	-0.05 (0.01)	11.1	6
	3	2.09 (0.07)	0.13 (0.03)	0.03 (0.01)	17.5	6
	4	2.23 (0.05)	0.18 (0.02)	0.10 (0.01)	16.1	6
	5	2.03 (0.05)	0.11 (0.01)	-0.01 (0.01)	10.8	5
	6	1.98 (0.04)	0.15 (0.01)	-0.06 (0.01)	10.9	5
	7	2.00 (0.05)	0.21 (0.02)	-0.05 (0.01)	9.4	5
	8	2.30 (0.05)	-0.03 (0.01)	0.02 (0.01)	1.7	5
	9	2.15 (0.07)	-0.05 (0.04)	0.01 (0.01)	7.4	5

Bibliography

1. Albright, A., C. Dixon and M. Hegedus. "Modification and Validation of Conceptual Design Aerodynamic Prediction Method HASC95 with VTXCHN." Report Prepared for Mike Logan at NASA Langley Research Center, CDAP-10, 1995.

2. Ames, Lawrence L. and Edward J. George. *Revision and Verification of a Seven-Point Workload Estimation Scale*. Air Force Flight Test Center Technical Information Memorandum. AFFTC-TIM-93-01. Edwards AFB CA, 1993.

3. Anderson, John D. Jr. *Fundamentals of Aerodynamics*. New York: McGraw-Hill Companies, 2001.

4. -----. *Introduction to Flight*. New York: McGraw-Hill Publishing Company, 1989.

5. Ashtech Surveying Systems. *Ashtech Z-Xtreme™ Operation and Reference Manual*. Thales Navigation: Santa Clara CA, June 2002.

6. Bertin, John J. *Aerodynamics for Engineers*. Saddle River, New Jersey: Prentice Hall, Inc., 2002.

7. Blake, William. Air Force Research Laboratory, Air Vehicles Directorate (AFRL/VACA), Wright Patterson AFB OH. Personal Interview. 8 April 2003.

8. Blake, William and Dieter Multhopp. "Design, Performance and Modeling Considerations for Close Formation Flight," *AIAA journal of Guidance, Control, and Dynamics*, AIAA-98-4343 (1998).

9. Brown, Frank A. Technical Expert for Aircraft Performance, Air Force Flight Test Center, Edwards AFB CA. Personal Interview. 18 October 2004.

10. Bruce, R. R. "KC-135R Aerodynamic Summary." Technical Drawing prepared for the Boeing Company, D458-40210. Seattle WA, 8 August 1972.

11. Cutts, C. J. and J. R. Speakman. "Energy Saving in Formation Flight of Pink-Footed Geese," *Journal of Experimental Biology*, 189: 251-261, 1994.

12. Department of the Air Force, *Combat Aircraft Fundamentals F-15 A/B/C/D*. AFM 3-3 Volume 4. Washington: HQ USAF, 17 September 1999.

13. Department of the Air Force. *Flight Manual USAF/EPAF Series Aircraft F-16A/B Blocks 10 and 15, Change 14*. T.O. 1F-16A-1. Washington: HQ USAF, 15 August 2003.

14. Department of the Air Force. *Supplemental Flight Manual, Change 10*. T.O. 1F-16A-1-1. Washington: HQ USAF, 15 February 2003.

15. F-16 Stability and Flight Control Analysis Group. "F-16 Block 15 Stability and Control Substantiation Report." General Dynamics, Fort Worth Division. CDRL#A025, 16PR1949. Fort Worth TX, September 1981.

16. Filiponne, A. "Heuristic Optimization Applied to an Intrinsically Difficult Problem -- Birds Formation Flight," *Aerospace Sciences Meeting and Exhibit, 34th.* AIAA-96-0515. Reno NV, 1996.

17. Hart, R. E. and W. H. Jones. *Performance, Flying Qualities, and Propulsion System Evaluation of the KC-135R Aircraft, Volume 2*. Air Force Flight Test Center Technical Report. AFFTC-TR-83-18. Edwards AFB CA, July 1983.

18. Hummel, Dietrich. "Aerodynamic Aspect of Formation Flight in Birds," *Journal of Experimental Biology*, Volume 104: 321-347 (1983).

19. -----. "The Use of Aircraft Wakes to Achieve Power Reductions in Formation Flight," *Proceedings of the AGARD FDP Symposium on "The Characterization and Modernization of Wakes from Lifting Vehicles in Fluid."* Trondheim, Norway, May 1996.

20. Lissaman, P. "The Facts of Lift," *Aerospace Sciences Meeting and Exhibit, 34th.* AIAA-96-0161. Reno NV, 1996.

21. Magill, Samantha A., Joseph A. Schetz and William H. Mason. "Compound Aircraft Transport: A Comparison of Wingtip-Docked and Close Formation Flight," *41st Aerospace Sciences Meeting and Exhibit.* AIAA-2003-0607. Reno NV, 2003.

22. Magill, Samantha A. and Wayne C. Durham. "Modelling and Simulation of Wingtip-Docked Flight," *Atmospheric Flight Mechanics Conference and Exhibit.* AIAA-2002-4493. Monterey CA, 2002.

23. Misra, Pratap and Per Enge. *Global Positioning System Signals, Measurement and Performance*. Lincoln, Massachusetts: Ganga-Jumana Press, 2001.

24. Moreno, Ian M. and others. “Limited Performance Evaluation of the F-16B.” Preliminary Report of Results to the Faculty of the USAF Test Pilot School, Edwards AFB CA, April 2004.

25. Morgan, Michael T. and others. *A Limited Investigation of Fuel Savings Associated With Close Formation Flight (Project Dollar Draft).* Air Force Flight Test Center Technical Information Memorandum. AFFTC-TIM-04-09. Edwards AFB CA, December 2004.

26. Munk, Max M. “The Minimum Induced Drag of Airfoils,” National Advisory Committee for Aeronautics (NACA) Report Number 121. 1921.

27. Nelson, Roger C. *Flight Stability and Automatic Control*. Boston: McGraw-Hill Companies, Inc., 1998.

28. Prandtl, L. “Induced Drag of Multiplanes.” National Advisory Committee for Aeronautics (NACA) Technical Notes Number 182. March 1924.

29. Reue, G. H. and R. H. Searle. “F-16 Aerodynamic Design Data Report, Appendix B.” General Dynamics, Fort Worth Division. CDRL#A027. Fort Worth TX, 3 October 1977.

30. Runnion, M. “VISTA/NF-16D Configuration Definition Study Report.” Prepared for AFWAL/FIGI Under CCP 4455, CDRL#9098. General Dynamics Corporation, Fort Worth Division, Fort Worth TX, 15 September 1998.

31. Simon, James M., Scott Lemay and Jay Brandon. “Results of Exploratory Wind Tunnel Tests of F-16/VISTA Forebody Vortex Control Devices.” Flight Dynamics Directorate Technical Report. WL-TR-93-3013. Wright-Patterson AFB OH, January 1993.

32. Technical Support Division, USAF Test Pilot School. “Airborne Instrumentation Handbook, Revision 5.0.” Edwards AFB CA: Air Force Flight Test Center, January 2004.

33. Vachon, M. Jake, Ronald J. Ray, Kevin R. Walsh, and Kimberly Ennix. “F/A-18 Aircraft Performance Benefits Measured During the Autonomous Formation Flight Project,” *Flight Mechanics Conference and Exhibit.* AIAA-2002-4491. Monterey CA, 2002.

34. Vlachos, Pavlos and Demetri Telionis. “Wing-Tip-to-Wing-Tip Aerodynamic Interference,” *41st Aerospace Sciences Meeting and Exhibit*. AIAA-2003-0609. Reno NV, 2003.

35. Wagner, Eugene H. *An Analytical Study of T-38 Drag Reduction in Tight Formation Flight*. MS Thesis, AFIT/GAE/ENY/02-2. School of Engineering and Management, Air Force Institute of Technology (AU), Wright-Patterson AFB, OH, March 2002 (ADA399875).

36. Waypoint Consulting, Inc. *GrafNav/GrafNet, GrafNav Lite, GrafMov, Inertial Explorer for Windows 95™, 98™, 200™, XP™ & NT™ Operating Manual Version 7.01*. Waypoint Consulting, Inc.: Calgary, Alberta, Canada, March 2004.

37. Webb, J. B. and S. A. Rudin. “Final F-16 Aerodynamic Status Report and Flight Test Results.” General Dynamics, Fort Worth Division, CDRL#A027, Fort Worth TX, 1 September 1999.

38. Weimerskirch, Henri, Julien Martin, Yannick Clerquin, Peggy Alexander, and Sarka Jiraskova. “Energy Saving in Flight Formation,” *Nature*, 413: 697-698 (18 October 2001).

Vita

Major Michael T. Morgan was born in Oscoda, Michigan. He graduated from Hopewell Area High School in Aliquippa, Pennsylvania in June 1990. He entered undergraduate studies at the United States Air Force Academy in Colorado Springs Colorado where he graduated with a Bachelor of Science degree in Aeronautical Engineering in June 1994 and was commissioned in the United States Air Force.

His first assignment was at Sheppard AFB, Texas as a student in Euro-NATO Joint-Jet Pilot Training. Upon graduating from pilot training in February 1996, he was assigned to the 20th Airlift Squadron at Travis AFB, California where he served as a pilot in the C-141 aircraft. In 1997 he was assigned to the 22nd Airlift Squadron at Travis AFB where he served as a pilot in the C-5 aircraft. In 1998, he was assigned to the 95th Fighter Training Squadron at Tyndall AFB, Florida where he was assigned as a student in the F-15C aircraft. In 1999, he was assigned to the 60th Fighter Squadron at Eglin AFB, Florida where he served as an F-15C pilot. In August 2002, he was selected to enter the USAF Test Pilot School in conjunction with the Air Force Institute of Technology. He graduated from the USAF Test Pilot School at Edwards AFB, California in December 2004. Upon graduation from AFIT, he will be assigned to the 40th Flight Test Squadron at Eglin AFB, Florida.

REPORT DOCUMENTATION PAGE

Form Approved
OMB No. 0704-0188

1. REPORT DATE *(DD-MM-YYYY)*	2. REPORT TYPE	3. DATES COVERED *(From - To)*
21-03-2005	Master's Thesis	September 2002 – March 2005

4. TITLE AND SUBTITLE

A Study In Drag Reduction of Close Formation Flight Accounting For Flight Control Trim Positions and Dissimilar Formations

5a. CONTRACT NUMBER

5b. GRANT NUMBER

5c. PROGRAM ELEMENT NUMBER

6. AUTHOR(S)

Morgan, Michael T., Major, USAF

5d. PROJECT NUMBER

5e. TASK NUMBER

5f. WORK UNIT NUMBER

7. PERFORMING ORGANIZATION NAME(S) AND ADDRESS(ES) AND ADDRESS(ES)

Air Force Institute of Technology
Graduate School of Engineering and Management (AFIT/EN)
2950 Hobson Way
Wright Patterson AFB OH 45433-7765

8. PERFORMING ORGANIZATION REPORT NUMBER

AFIT/GAE/ENY/05-M13

9. SPONSORING / MONITORING AGENCY NAME(S) AND ADDRESS(ES)

United States Air Force Test Pilot School (USAF TPS)
Attn: Maj. Russell G. Adelgren
220 S. Wolfe Ave.
Edwards AFB, CA 93523 DSN: 277-3000

10. SPONSOR/MONITOR'S ACRONYM(S)

11. SPONSOR/MONITOR'S REPORT NUMBER(S)

12. DISTRIBUTION / AVAILABILITY STATEMENT

APPROVED FOR PUBLIC RELEASE; DISTRIBUTION UNLIMITED.

13. SUPPLEMENTARY NOTES

14. ABSTRACT

The purpose of this research was to further define the position of maximum benefit for the wingman of a two-ship formation of aircraft. An analytical analysis was conducted using a vortex lattice code. Investigations of a similar formation of F-16 aircraft and a dissimilar formation with a KC-135 lead aircraft and F-16 trail aircraft were conducted. The analysis determined the effects of varying airspeed on the optimal position. Additionally, the flight control surface deflections were taken account during the analyses, and the flight control positions were determined to be within the bounds of the F-16 aircraft. The similar formation profile was further investigated during flight test. The flight test investigated the change in vertical positioning as well as lateral spacing from the analytic analysis. The drag savings profile has the capability to increase the range of existing airframes, providing the benefit at no cost.

15. SUBJECT TERMS

Flight Test, Formation Flight, Vortex, Vortex Wake Effects, Aerodynamic Wake, Fuel Conservation, Drag, Drag Reduction

16. SECURITY CLASSIFICATION OF:			17. LIMITATION OF ABSTRACT	18. NUMBER OF PAGES	19a. NAME OF RESPONSIBLE PERSON
					David R. Jacques, Dr. (SYE)
a. REPORT	b. ABSTRACT	c. THIS PAGE			19b. TELEPHONE NUMBER *(include area code)*
U	U	U	UU	132	(937) 255-7777, ext 3329; e-mail: David.Jacques@afit.edu

Standard Form 298 (Rev. 8-98)
Prescribed by ANSI Std. Z39.18